UNIVERSITY OF CENTRAL FLORIDA
DISSERTATION APPROVAL

Date October 24, 1996

I hereby recommend that the dissertation prepared and successfully defended under my supervision entitled: Approximate Trigonometric Expansions with Applications to Signal Decomposition and Coding

by Qurban A. Memon

be accepted in partial fulfillment of the requirements for the degree of

Doctor of Philosophy

from the Department of Electrical and Computer Engineering, College of Engineering.

Takis Kasparis, Chair

Nicholaos S. Tzannes

Wasfy B. Mikhael

Michael G. Georgiopoulos

Mubarak A. Shah

Wasfy B. Mikhael
Department Chair

Jose A. Sepulveda
Graduate Coordinator

Martin P. Wanielista
Dean

Diane M. Jacobs
Vice President for Research and
Graduate Studies

FINAL EXAMINATION COMMITTEE

The material presented within this report does not necessarily reflect the opinion of the committee, the College, or the University of Central Florida.

APPROXIMATE TRIGONOMETRIC EXPANSIONS WITH APPLICATIONS TO SIGNAL DECOMPOSITION AND CODING

by

QURBAN A. MEMON

M.E. University of Florida, Gainesville, 1993

A dissertation submitted in partial fulfillment of the requirements
for the degree of Doctor of Philosophy in Engineering
in the Department of Electrical and Computer Engineering
in the College of Engineering
at the University of Central Florida
Orlando, Florida

Fall Term
1996

Major Professor: Takis Kasparis

ABSTRACT

Signal representation and data coding for multidimensional signals have recently received considerable attention due to their importance to several modern technologies. Many useful contributions have been reported that employ wavelets and transform methods. For signal representation, it is always desired that a signal be represented using minimum number of parameters. The transform efficiency and ease of its implementation are to a large extent mutually incompatible. If a stationary process is not periodic, then the coefficients of its Fourier expansion are not uncorrelated. With the exception of periodic signals the expansion of such a process as a superposition of exponentials, particularly in the study of linear systems, needs no elaboration. In this research, stationary and non-periodic signals are represented using approximate trigonometric expansions. These expansions have a user-defined parameter which can be used for making the transformation a signal decomposition tool. It is shown that fast implementation of these expansions is possible using wavelets. These approximate trigonometric expansions are applied to multidimensional signals in a constrained environment where dominant coefficients of the expansion are retained and insignificant ones are set to zero. The signal is then reconstructed using these limited set of coefficients, thus leading to compression. Sample results for representating multidimensional signals are given to illustrate the efficiency of the proposed method. It is verified that for a given a number of coefficients, the proposed technique yields higher signal to noise ratio than conventional techniques employing the discrete cosine transform technique.

ACKNOWLEDGEMENT

I would like to express my sincere appreciation and gratitude to my advisor and chairman of my supervisory committee, Dr. Takis Kasparis for his guidance and support throughout the course of my doctoral studies and research. I wish to thank my committee members Dr. Mubarak A. Shah, Dr. Michael N. Georgiopoulos, and Dr. Wasfy Mikhael for their help and participation in my supervisory committee.

My special thanks to my doctoral program supervisory committee member Dr. Nicholaos Tzannes for his technical suggestions and pointing out this topic of research.

I would also wish to thank my friends Khizar Farooq, Muhammad A. Ibrahim, Hasan Appadwedulla, Louay Rukieh, and Ashfaq Khan for fruitful discussions and suggestions. Finally I wish to thank my parents, brothers, and cousins for raising me to appreciate the value of learning and for building in me those qualities necessary for the completion of a task such as this.

TABLE OF CONTENTS

TABLE OF FIGURES

LIST OF TABLES

1 . INTRODUCTION

1.1 Background

The use of digital data has increased at a rapid pace over the past decade. Digital signal and image processing generally creates significant number of large files containing digital data. Very often, these must be archived or exchanged among different users and systems. Computer-generated data has become an extensive source of digital data, particularly for special effects in advertising and entertainment. In case of digital images, the reason is obvious: representing images in digital form allows visual information to be easily manipulated in useful and novel ways. Computers' emerging ability to manipulate and display images and video increases their information-handling potential by orders of magnitude. As the computers' utility as an information source grows, it opens a host of applications opportunities in communications, education, and image archiving. The multimedia market is characterized by numerous manufacturers, each using its own technology for digital audio and video, script languages, communication protocols, operating system extensions, and so on. Hardware limitations can stand in the way of implementing these applications in different environments. Thus, it has become necessary to find efficient representations for digital data in order to reduce the memory required for storage, improve the data access rate from storage devices, and reduce the band-width and/or time required for transfer across communication channels. The key that unlocks the potential of computer-based video is digital compression. In the literature, the terms source coding,

digital coding, data compression, band-width compression, and signal compression are all used to connote the function of achieving a compact digital representation of a signal, including the important subclass of analog signals such as speech, audio, and image. A wide range of techniques have emerged in the recent past and new techniques continue to emerge for efficient storage and transfer of digital data. Data compression techniques exploit redundancy and irrelevance by transforming a data file into a smaller file from which the original file can later be reconstructed, exactly or approximately. The ratio of the two file sizes specifies the degree of compaction or compression ratio. The times required for file compression are not negligible. The algorithms that achieve the densest compaction are not usually the fastest, so choices must be made for each application. This chapter is divided into four main sections. In section 1.2, we present overview of information theory and concepts. Section 1.3 presents classification of compression techniques. In section 1.4, we present scope of this dissertation.

1.2 Information Theory and Concepts

Information theory gives some important concepts that are useful in digital representation of signals. Some of these concepts are used in image quantization, image transforms and image data compression.

Suppose we have a memoryless source of messages that uses an alphabet $\{a_k\}, k = 0, 1, .., K-1$ where K is total number symbols in that alphabet with a_k being the symbols. Suppose further that the probability of occurrence of each symbol is known and denoted as $P(a_k)$. In a message from a memoryless source, the ordering of the symbols in the message is unimportant; only their presence in the message matters. Shannon [1,2]

defined a measure of the information imparted by the occurrence of the symbol a_k in a message as:

$$I(a_k) = -\log[P(a_k)] \tag{1.1}$$

This definition implies that the information conveyed is large when an unlikely message is generated. The entropy of the message source, defined by:

$$H = E\{I(a_k)\} = -\sum_{k=0}^{K-1} P(a_k)\log[P(a_k)] \tag{1.2}$$

specifies the average information content (per symbol) of the messages generated by the source. If we choose 2 as the base for the logarithm, the units of entropy are *bits per symbol.* A coding scheme removes all redundancy from the message if it produces an average word length that is equal to the entropy of the message source. The concept of memoryless source is too restrictive for most practical purposes. Instead a source with memory is often used. Such a source is known as Markov process. A *p*th order Markov process is a source in which the probability of occurrence of a source symbol a_k depends upon a finite number p of preceding symbols. It is also useful to associate the Markov process with some state, which depends on preceding p symbols.

According to Shannon's noiseless coding theorem [3,4], it is possible to code without distortion a source of entropy H bits using an average of $H + \varepsilon$ bits/message, where $\varepsilon > 0$ is an arbitrarily small quantity. An alternative form of this theorem states that it is possible to code the source with H bits such that the distortion in the decoded message could be made arbitrarily small. While the noiseless coding theorem provides the extension of a code that can achieve the rate approaching the source entropy, it however does not provide the code. Generally, variable length codes are employed with source extensions to reach the desired

performance. Some of the known techniques are Shannon-Fano, Huffman and modified Huffman coding techniques.

In analog-to-digital conversion of data, it is inevitable that the digitized data would have some error, however small, when compared to analog sample. Rate distortion theory provides some useful results, which tell us the minimum number of bits required to encode the data, while admitting a certain level of distortion and vice versa. Intuitively, we expect that, the more information we transmit, the better the reproduced quality will be. As a simple example, consider the operation of quantization using differing accuracies (number of bits). Clearly, if we decide to quantize with an accuracy of 10 bits, the approximate version of the signal will be much closer to the original signal than if we choose a 3-bit quantizer. However, in any given sampling interval, we pay the penalty (in terms of transmission capacity) of having to transmit ten digits instead of three to achieve the higher quality. In general, the central region of the curve relating rate and distortion will have a negative slope, as shown in Fig. 1.1. For very low rates of information transmission, the distortion reaches a maximum value D_{max}, which in case of continuous distribution, will be total signal energy. Clearly, if the allowable distortion in the received signal is equal to the signal energy, then we may as well not bother to transmit the signal at all, and the rate will then be zero. At the other end of the distortion scale, as we require better and better reproduced signal quality (lower and lower distortion), then the rate must increase and, in the continuous case, become infinite if perfect reproduction is desired.

1.3 Classification of Compression Techniques

Signal compression plays a crucial role in many important and diverse applications, including video teleconferencing, remote sensing, document and medical imaging, facsmile transmission, and the control of remotely piloted vehicle applications. The purpose of data compression is to remove different redundancies such as statistical redundancy and subjective redundancy from the data so that it takes less time to transmit and less space to store. From mathematical point of view, statistical redundancy amounts to transforming a data array into a statistically uncorrelated data set. Subjective redundancy, on the other hand, can be used to reduce transmission bit rate by using a number of bits that are necessary for subjectively acceptable signal quality at the receiver. There are many approaches to compression. However, they can be categorized into two main groups: *lossless* and *lossy*. Fig. 1.2 depicts three basic components of a general compression scheme: (1) signal decomposition or transformation, (2) quantization, and (3) symbol encoding. The signal decomposition is usually a reversible operation and is performed to eliminate redundant information from the data. This stage is used in both lossless and lossy techniques. The next stage, quantization, is a many-to-one mapping found only in lossy techniques, and it is the point where errors are introduced. The type or degree of quantization has a large impact on the bit rate and the reconstructed signal quality of a lossy scheme. Examples of quantization strategies include uniform or nonuniform scalar quantization or vector quantization. The final stage is a means for mapping the symbols (values) resulting from decomposition and/or quantization stages into a strings of 0's and 1's, which then can be transmitted or stored. This mapping may be as simple as using fixed-length code, such as a Huffman code or an arithmetic code, as a means of achieving rates close to the fundamental information-theoretic

limits. The three components shown in Fig. 1.2 often mutually interact, and their joint optimization is a complicated task. As a result, they are often optimized individually based on assumed inputs.

1.3.1 Lossless Compression

In lossless compression also known as reversible compression, the reconstructed signal is numerically identical to the original signal on sample to sample basis. This compression scheme is ideal since no information is compromised, but the amount of compression achieved is much less than lossy compression. Some compression applications require the reconstructed signal to be lossless. Some examples are seismic signals, and medical imaging applications where diagnostic accuracy can not be compromised. Lossless data compression algorithms fall into two broad categories: dictionary-based techniques and statistical methods.

Dictionary-based techniques generate a compressed file containing fixed-length codes (usually 12 to 16 bits), each of which represents a particular sequence of bytes in the original file. Some of the commonly used dictionary-based data compression techniques are run-length encoding (RLE) and Lemple, Ziv and Walsh (LZW) algorithm. RLE achieves considerable compaction when used on images having few gray levels or images of objects residing on constant background. In an image being stored line by line, a series of pixels having the same gray-level value is called a *run*. One can store a code specifying that value, followed by the length of the run, rather than simply storing the same value many times over. This is run-length encoding. Under worst conditions (for example, where every pixel differs from its neighbors) RLE can actually double the size of the file. LZW technique is

an extended version of original LZ technique first described by Lemple and Ziv [5,6]. Like RLE, it effects compression by encoding strings of characters. However, unlike RLE, it builds up a table of strings (particular sequence of bytes) and their corresponding codes as it encodes the file. The first time a string not already in the table occurs, it is stored in full, along with the code that is assigned to it. Thereafter, when that string occurs again, only its code is stored. This squeezes redundancy out of the file. A file of 8-bit bytes can be encoded, for example, into 12-bit codes. Of the 4,096 possible codes, 256 of them represent all possible single bytes. The remaining 3,840 are assigned to strings as they are encountered in the data during compression. Not only is the string table built dynamically during compression, but it need not be stored with the compressed file. The decompression algorithm can reconstruct string table from the information in the compressed file.

Statistical methods implement data compression by representing frequently occurring characters in the file with fewer bits than they do less commonly occurring ones. Huffman coding[7], introduced in the 1950s, is a lossless statistical method that always finds a variable-length code with minimum redundancy. It uses a binary encoding tree for representing commonly occurring values in few bits and less common values in more bits. Dynamic Huffman coding constructs the encoding tree on the fly, during the compression process[8]. More advanced statistical methods [9-10] can achieve higher compression ratios, but at the cost of increased encoding and decoding times.

Apart from two main lossless compression categories discussed briefly above, there are other techniques such as:

1. Bit plane coding: Consider a signal where each sample is represented by K bits. By selecting a bit from each position of a binary representation of each sample, a binary signal

called bit plane is created, thus decomposing the entire signal into K planes. Each of these planes can then be encoded using a lossless binary compression technique such as Joint Bi-level Information Group (JBIG), Gray codes, run length codes or adaptive binary arithmetic coder such as Q-coder.

2. Predictive Coding: This coding technique uses correlation between adjacent samples. Here attempt is made to predict the value of a given sample based on the value of its previous neighbors. In theory, lossless coding technique is capable of encoding a signal at a bit rate close to its entropy. A practical implementation of this general approach is called lossless differential pulse code modulation (DPCM).

1.3.2 Lossy Compression

In lossy compression also known as irreversible compression, the degradations are allowed in exchange for a reduced bit rate. As a result much higher compression ratios can be achieved as compared to lossless compression. It is important to note that these degradations may or may not be visually apparent. Some of the most common lossy compression techniques include:

1. Predictive Coding
2. Subband Coding
3. Transform Coding

Predictive coding, carried out in the spatial (data) domain, is statistical in nature and mainly based on the assumption that the signal elements in the same neighborhood tend to have similar amplitudes. We may therefore, use the value(s) of one or more earlier elements (which have been previously coded) to form a prediction of the present element. This pre-

dicted value is subtracted from the actual value of the present element. This difference is then coded and transmitted or stored. The entire signal is reconstructed by adding the difference signal to the prediction carried out in the decoder. This scheme is shown in Fig. 1.3. The only error (ignoring external channel effects) involved is in quantizing the difference signal. This technique, however, is sensitive to variations in input data statistics and also to channel errors.

Transform coding which is a, loosely speaking, a frequency domain process, is also statistical in nature. Transform coding is one of the well known approaches to efficient waveform representation at medium to low bit rates. To what extent a particular transform will support data compression depends upon both the transform and the nature of the images being compressed. The practicality of an image coding scheme depends on the computational work load of the encoding and decoding steps, as well as the degree of compression obtained. The availability of a fast implementation algorithm can greatly enhance the appeal of a particular transform. The goal of transform coding is to decorrelate the signal, resulting in the energy being distributed among only a small set of coefficients. In this way, many coefficients can be discarded after quantization and prior to encoding. A transformation can be viewed as a decomposition of the original block of signal into a set of basis functions. In case of sinusoidal transforms (such as Fourier transform), the basis functions consist of sines and/or cosines with different spatial frequencies, and each transform coefficient is proportional to the fraction of energy in the original block at that particular frequency. It is important to realize that the transform operation by itself does not achieve any compression, but by changing the representation of the information contained in the signal block, it makes the data more suitable for compression. Compression is achieved by subsequent steps of

quantization and encoding of the transform coefficients. Input-dependent transforms are hard to implement, but they also have the best input decorrelating and variance ordering properties. A practical transform for the purpose of signal compression should have a strong decorrelating effect, should preferably consist of signal-independent basis functions, and should have a fast implementation. Combined with other compression techniques, signal transforms allow the transmission, storage, and display of images and video sequences that otherwise would be impractical.

The uneven distribution of signal energy in frequency domain has made signal decomposition an important practical problem. The recent activity in signal decomposition is driven by signal processing and coding applications. More recently, the wavelet transform with a capability for variable time-frequency resolution has gained a considerable attention as an elegant multiresolution signal processing tool. The basic concept is to divide the signal spectrum into its subbands and, then, to treat those subbands individually for the purpose of signal representation or coding. This technique has two desirable features. First, monitoring of signal energy within subbands is possible and then the subbands can be ranked and processed independently. Second, the subband decomposition leads to multiresolution signal decomposition of the signal spectrum. The signal can thus be represented at each resolution. Therefore, the basic objective in signal analysis is to devise a transformation that represents a signal features simultaneously in time and frequency.

There are other lossy compression techniques such as block truncation coding and vector quantization. The most commonly used error measures are root mean square error (RMSE) and signal to noise ratio (SNR). It should however be noted that small RMSE or higher SNR does not necessarily mean better subjective quality of reconstructed signals.

1.3.3 Compression Standardization Activities

Digital video coding technology has developed into a mature field and a diversity of products has been developed targeted for a wide range of emerging applications, such as video on demand, digital TV/HDTV broadcasting, and multimedia image/video database services. With the increased commercial interest in video communications the need for international image and video coding standards arose. Standardization of video coding algorithms holds the promise of large markets for video communication equipment. From the beginning of 1980's, standardization activities started within CCITT, followed by CCIR and ISO later on. The outcome of these activities are CCITT Recommendations H.120 and H.261, CCIR Recommendations 721 and 723, ISO 10918 (JPEG), and ISO 11721 (MPEG-1). ISO 13818 (MPEG-2) has just been drafted and ISO MPEG-4 is in its developing phase. The JPEG and MPEG standards both describe the content of information objects only. They cannot describe the interrelationship between the different pieces of a multimedia presentation. The definition and standardization of such structure information is the purpose of the Multimedia and Hypermedia Information Coding Experts Group (MHEG).

Since the aim of standardization is to foster implementations of image and video coding equipment, the capability of current state-of-art technology needs to be taken into account. Therefore, international standards do not necessarily represent the basic technical solutions, but rather attempt to achieve a compromise between the amount of flexibility supported by the standard, the implementation complexity required and compression efficiency achieved. In this section, we briefly describe JPEG, MPEG standards.

1.3.3.1 Joint Photographics Experts Group (JPEG)

The Joint Photographics Experts Group (JPEG), sponsored jointly by the International Standards Organization (ISO) and CCITT, has established an open (published, non-proprietary) algorithm for compression of still images[11]. It achieves compression ratios of 15-25 without a significant loss of visual quality. With a slight sacrifice of quality, 40-to-1 compression, or more, is possible. The JPEG standard includes two basic compression methods, each with various modes of operation. A DCT based method is specified for lossy compression, and a predictive method for lossless compression.

JPEG, to meet the requirement for a lossless mode of operation, has chosen a simple predictive method. A predictor combines the value of up to three neighboring samples (A, B, and C) to form a prediction of the sample indicated by X in Fig. 1.4. The prediction is then subtracted from the actual value of sample X, and the difference is encoded without any loss by either of the entropy coding methods-Huffman or arithmetic. The eight predictors are listed in Table 1.1. Selections 1,2, and 3 are 1-D predictors and selections 4,5,6, and 7 are two dimensional predictors. Lossless codecs typically produce 2:1 compression for images with moderately complex scenes.

The following is the brief outline of JPEG baseline method[12]. Fig. 1.5. Shows simplified block diagram of JPEG encoder and decoder. JPEG encoder is straight forward. It converts image detail to a spatial frequency representation using a 2-D discrete cosine transform (DCT). It quantizes the components with different degrees of granularity, reflecting the human visual system's spatial frequency sensitivity, then encoding using variable length (entropy) coding. JPEG decoder, on the other hand, does the reverse process for reconstruction.

If the image is in color, the JPEG algorithm first converts from RGB components to luminance and chrominance components and discards half the chrominance information. Then it uses the DCT for block transform coding, discards high-frequency coefficients, and quantizes the remaining coefficients to reduce the data volume further. Finally, it applies RLE and Huffman coding to finish the compression task. JPEG decompression is simply the reverse of JPEG compression, making the algorithm symmetrical.

1.3.3.2 Moving Pictures Experts Group (MPEG)

An open algorithm, developed by the Motion Picture Experts Group (MPEG), compresses full-motion video (motion pictures with sound). It is similar in concept to the JPEG algorithm, except that it also exploits the redundancy between consecutive video frames. The resulting compression ratios of 100:1 make it practical for transmitting color video with sound over one mega bit per second channels and storing digital video clips of reasonable duration on disk drives[13]. The basic idea is to apply JPEG to specific frames called *I* frames and then prediction based techniques in the temporal direction. This produces the *B* and *P* frames. The prediction also incorporates motion compensation for better efficiency. A given image's prediction may be based on future images as well as past ones, so the encoder must reorder images to put reference images before the predicted ones. The decoder puts the images back into display order. MPEG-1 is frame based and aims at bit rates 0.5-1.5 Mbits/sec. The MPEG-2 incorporates the concept of scalability. It is field based and aims at bit rates up to 15 Mbits/sec. Basically, MPEG-2 can be seen as a superset of the MPEG-1 coding standard and was designed to be backward compatible to MPEG-1 i.e., every MPEG-2 compatible can decode a valid MPEG-1 bit stream. MPEG-4 started its activities

in July 1993 with the charter to develop a generic video coding algorithm mainly targeted for a wide range of low bit rate multimedia applications. A wide range of algorithms are currently discussed as possible candidates for the future MPEG-4 and H.263/L standards. Many of the algorithms are based on so-called "second-generation coding techniques" for example object oriented based coding schemes, model based coding techniques, and segmentation based coding techniques. Many of the schemes divert significantly from successful hybrid DCT/DPCM coding concept employed in the current H.261, MPEG-1, and MPEG-2 standards.

1.4 Scope of Dissertation

The dissertation is organized as follows:

In chapter 2, we present an approximate Fourier expansion (AFE) of 1-D sampled, stationary and non-periodic signals. Furthermore, some mathematical properties of the expansion are derived along with error analysis. Additionally, we extend this expansion to an approximate cosine expansion (ACE) and show that for purposes of data compression with minimum error reconstruction of 1-D signals, the performance of ACE is better than AFE. The performance of this technique is compared with existing orthogonal transform techniques.

In chapter 3, we explore the capability of an approximate Fourier expansion (AFE) as signal decomposition tool. This expansion has a user-defined parameter which can be used for multiresolution decomposition of the signal. In this section, 1-D signals and images will be decomposed using an approximate Fourier expansion (AFE), and later these decomposed signals can be represented using an approximate cosine expansion (ACE). Signal, thus, is

represented at each resolution. Furthermore, the transformation efficiency of these approximate trigonometric expansions will be analyzed using first order Markov process and compared with existing techniques. Simulation results will be presented and compared with single transform alone and using a single transform in conjunction with wavelets.

In chapter 4, we apply and test an approximate Fourier expansion (AFE) to images and multispectral imagery. In order to apply this technique to multidimensional signals such as images and multispectral imagery, we test and compare the capability of these expansions with existing 2-D signal coding techniques. Furthermore, this technique is applied to images and multispectral imagery for coding purposes. Simulation results will also be presented.

In chapter 5, we present conclusions of this research. Recommendations for further research are also presented.

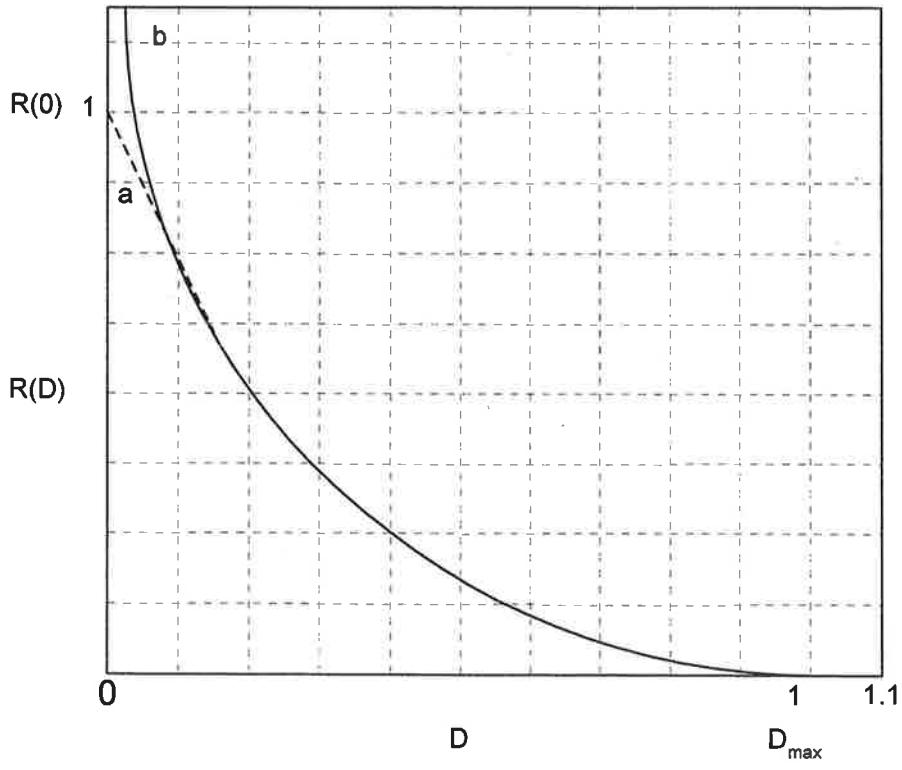

Fig. 1.1 General form of the rate distortion relation R(D) (a) Discrete Case (b) Continuous case

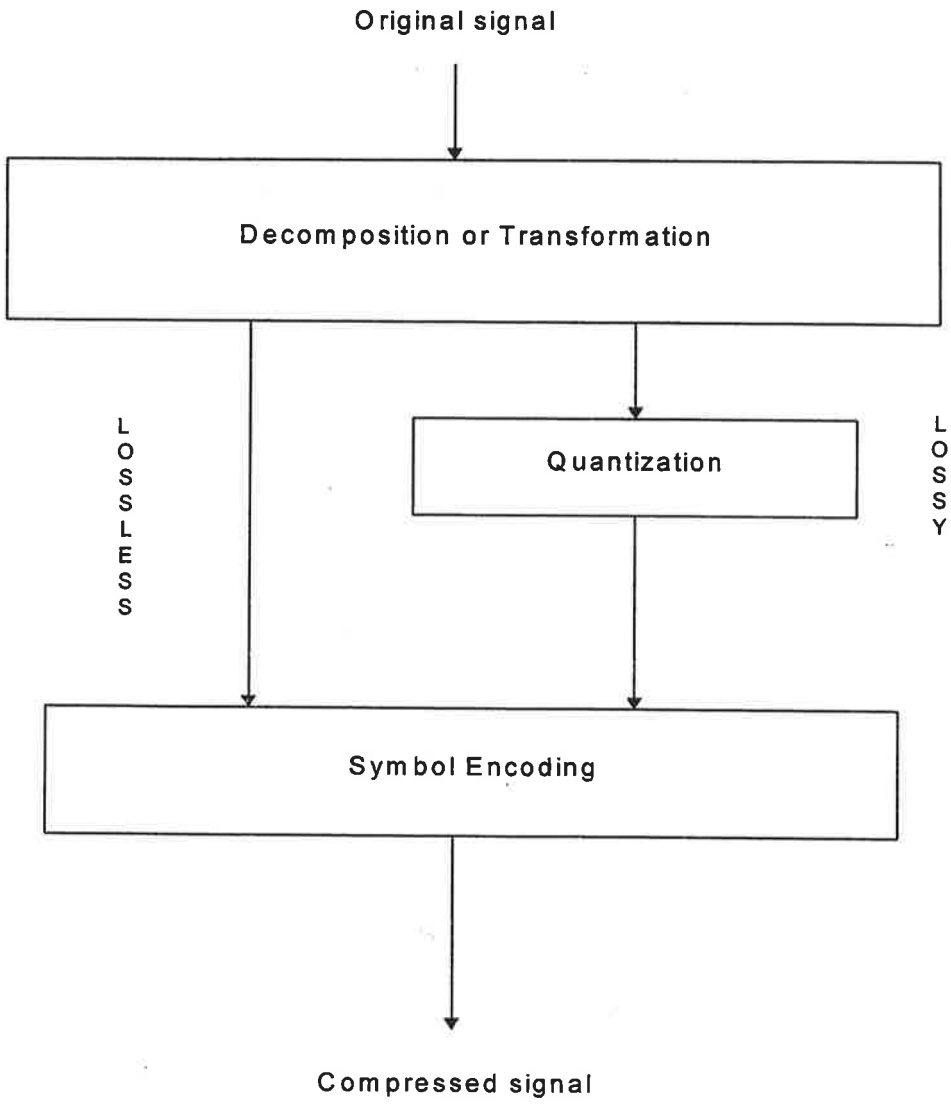

Fig. 1.2 General compression framework

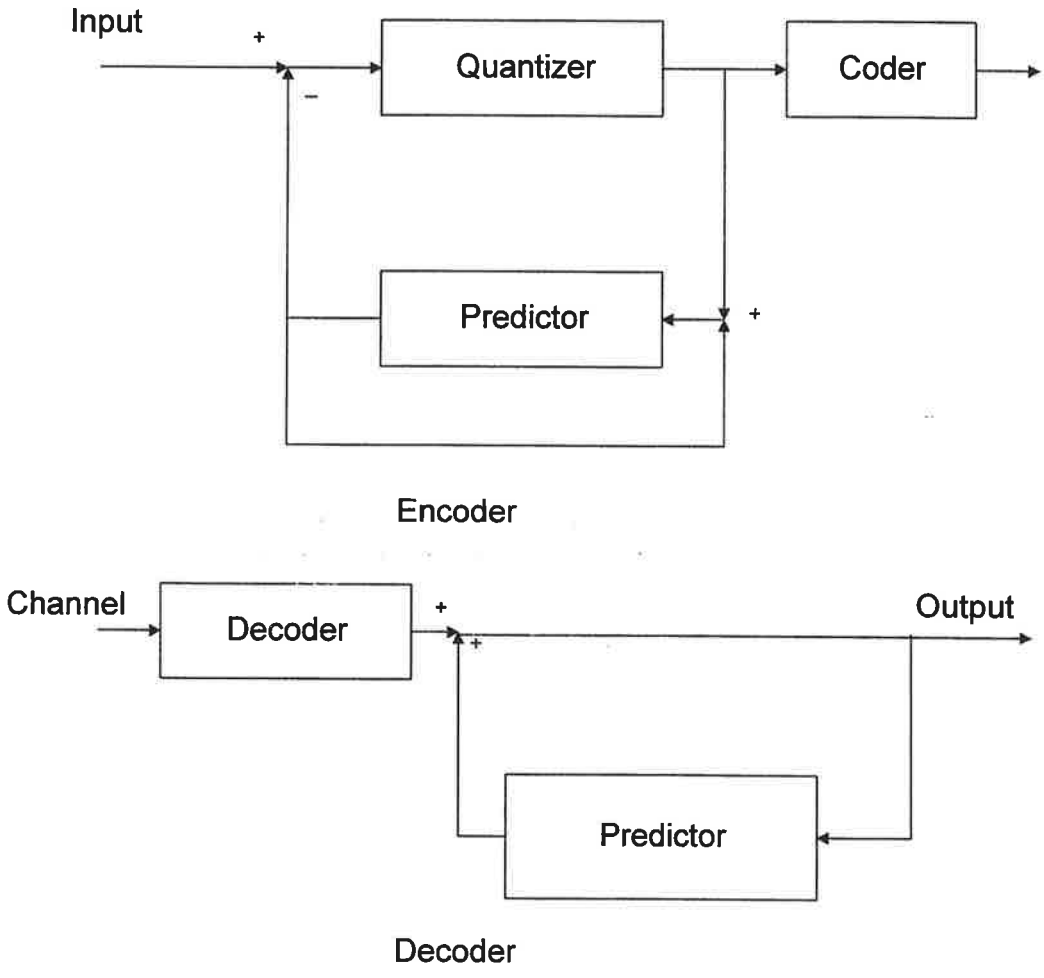

Fig. 1.3. Lossy DPCM encoder and decoder

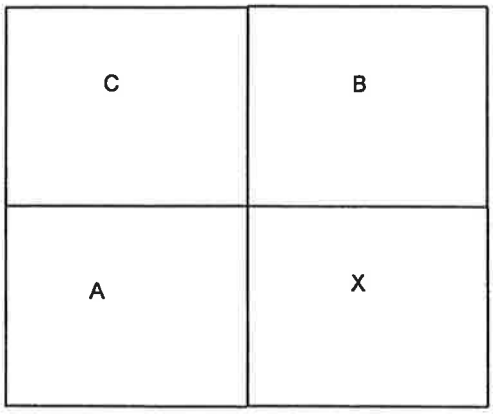

Fig. 1.4. JPEG lossless prediction

Value	Prediction
0	No Prediction
1	A
2	B
3	C
4	A+B+C
5	A+((B-C)/2)
6	B+((A-C)/2)
7	(A+B)/2

Tabel 1.1. JPEG predictors for lossless coding

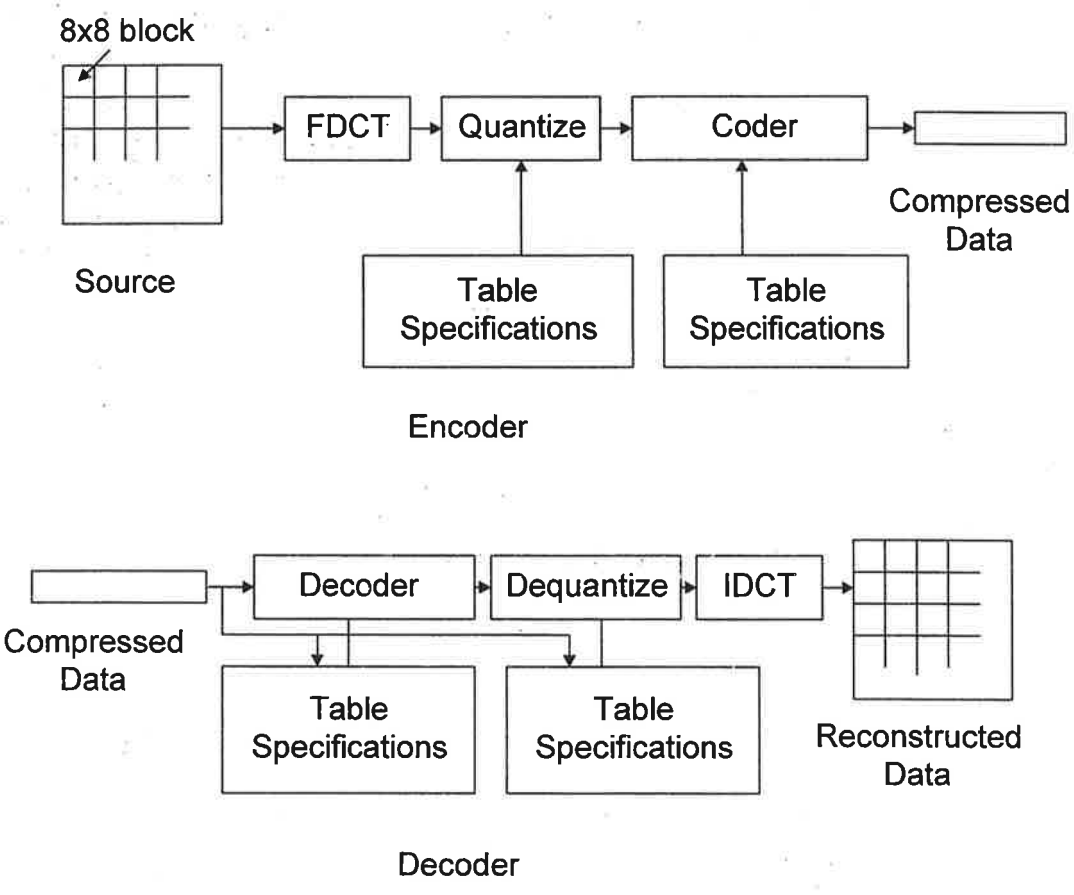

Fig. 1.5. Block diagram of JPEG encoder and decoder

2. SIGNAL REPRESENTATION USING THE APPROXIMATE TRIGONOMETRIC EXPANSIONS

2.1 Introduction

With the continuing growth of modern communications technology, demand for data storage and transmission is increasing rapidly. The efficiency, complexity as well implementation of a compression algorithm are particularly important in its hardware implementation. Transform coding is one of the well known approaches to efficient waveform representation at medium to low bit rates. The goal of transform coding is to decorrelate the signal, resulting in the energy being distributed among only a small set of coefficients. In this way, many coefficients can be discarded after quantization and prior to encoding. A transformation can be viewed as a decomposition of the original block of signal into a set of basis functions. In case of sinusoidal transforms (such as Fourier transform), the basis functions consist of sines and/or cosines with different spatial frequencies, and each transform coefficient is proportional to the fraction of energy in the original block at that particular frequency. It is important to realize that the transform operation by itself does not achieve any compression, but by changing the representation of the information contained in the signal block, it makes the data more suitable for compression. Compression is achieved by subsequent steps of quantization and encoding of the transform coefficients. The optimal decorrelation transformation is the Karhunen-Loeve transform (KLT)[14]. The KLT has the property that for any integer $L \leq N$, where L is the size of the transform and N is the size of data vector, it packs the maximum average energy into some L coefficients[15]. Unfortunately, no efficient computation of KLT exists, and also it does not have desirable prop-

erties of trigonometric series. Another complication in applying KLT is that its basis functions are not fixed, but are data dependent. Input-dependent transforms are hard to implement, but they also have the best input decorrelating and variance ordering properties. A practical transform for the purpose of signal compression should have a strong decorrelating effect, should preferably consist of signal-independent basis functions, and should have a fast implementation. For stationary random sequences there are other unitary transforms which approach to energy packing efficiency of the KLT. Examples are discrete cosine, Fourier and sine transforms. These transforms are members of a large family of sinusoidal transforms all of which have a performance equivalent to KLT as the size N of the data vector approaches infinity[16].

Consider a stationary process $x(t)$ with autocorrelation $R_x(\tau)$ and power spectrum $S_x(\omega)$. If $x(t)$ is periodic with period T (and so is the $R_x(\tau)$ with period T) then the process $x(t)$ can be expanded into Fourier series[17] as:

$$x(t) = \sum_{k=-\infty}^{\infty} c_k e^{jk\omega_o t}, \qquad \omega_o = \frac{2\pi}{T} \tag{2.1}$$

where the coefficients c_k are orthogonal (and uncorrelated) random variables, and are given by:

$$c_k = \frac{1}{T}\int_{-\frac{T}{2}}^{\frac{T}{2}} x(t) e^{-jk\omega_o t}\, dt \tag{2.2}$$

and their variance is related to the series expressions:

$$R_x(\tau) = \sum_{n=-\infty}^{\infty} \alpha_k e^{jk\omega_o \tau}, \qquad S_x(\omega) = 2\pi \sum_{k=-\infty}^{\infty} \alpha_k \delta(\omega - k\omega_o) \quad \text{where} \quad \alpha_k = E\{|c_k|^2\} \tag{2.3}$$

We will now show that if $R_x(\tau)$ is not periodic then the coefficients are no longer orthogonal. To prove this, we expand $R_x(\tau - t)$ in a Fourier series in the interval $\left(-\frac{T}{2}, \frac{T}{2}\right)$ as:

$$R_x(\tau - t) = \sum_{n=-\infty}^{\infty} \beta_k(t) e^{jk\omega_o \tau} \qquad |\tau| < \frac{T}{2} \tag{2.4}$$

where $\beta_k(t)$ is given by:

$$\beta_k(t) = \frac{1}{T} \int_{-\frac{T}{2}}^{\frac{T}{2}} R_x(\tau - t) e^{-jk\omega_o \tau} d\tau \tag{2.5}$$

From (2.2) we have:

$$c_k x^*(t) = \frac{1}{T} \int_{-\frac{T}{2}}^{\frac{T}{2}} x(\tau) x^*(t) e^{-jk\omega_o \tau} d\tau$$

Taking expected values, we obtain:

$$E\{c_k x^*(t)\} = \frac{1}{T} \int_{-\frac{T}{2}}^{\frac{T}{2}} E\{x(\tau) x^*(t)\} e^{-jk\omega_o \tau} d\tau = \frac{1}{T} \int_{-\frac{T}{2}}^{\frac{T}{2}} R_x(\tau - t) e^{-jk\omega_o \tau} d\tau = \beta_k(t) \tag{2.6}$$

Using (2.2) we can also write:

$$c_k c_m^* = \frac{1}{T} \int_{-\frac{T}{2}}^{\frac{T}{2}} c_k x^*(t) e^{jm\omega_o t} dt$$

Taking expected values and using the result from (2.6), we get:

$$E\{c_k c_m^*\} = \frac{1}{T} \int_{-\frac{T}{2}}^{\frac{T}{2}} E\{c_k x^*(t)\} e^{jm\omega_o t} dt = \frac{1}{T} \int_{-\frac{T}{2}}^{\frac{T}{2}} \beta_k(t) e^{jm\omega_o t} dt \tag{2.7}$$

i.e., the expected value of $c_k c_m^*$ equals the mth coefficient in the Fourier series expansion of the function $\beta_k(t)$. If $R_x(\tau)$ is periodic with period T, then $R_x(\tau)$ in equation (2.3) can be written as:

$$R_x(\tau - t) = \sum_{k=-\infty}^{\infty} \alpha_k e^{jk\omega_o(\tau - t)}$$

Putting this value in (2.5), we get:

$$\beta_k(t) = \frac{1}{T} \int_{-T/2}^{T/2} \alpha_k e^{jk\omega_o(\tau - t)} e^{-jk\omega_o \tau} d\tau = \alpha_k e^{-jk\omega_o t}$$

In this case, the equation (2.7) becomes:

$$E\{c_k c_m^*\} = \frac{1}{T} \int_{-\frac{T}{2}}^{\frac{T}{2}} \alpha_k e^{-jk\omega_o t} e^{jm\omega_o t} dt = \begin{cases} \alpha_k & if \quad k = m \\ 0 & if \quad k \neq m \end{cases} \tag{2.8}$$

If $R_x(\tau)$ is not periodic, then the coefficients c_k are no longer orthogonal but the expected value of $c_k c_m^*$ equals the mth coefficient in the Fourier series expansion of the function $\beta_k(t)$ (see equation 2.7). It can be shown that if $T \rightarrow \infty$ then c_k are approximately uncorrelated. If we replace the limits of integration in (2.5) by $\pm\infty$ we commit an error that is small for large T i.e., using equation (2.6), we get:

$$T\beta_k(t) = \int_{-\infty}^{\infty} R_x(\tau - t) e^{-jk\omega_o \tau} d\tau + \varepsilon(t, T)$$

Let $\tau - t = t'$ so that

$$T\beta_k(t) = e^{-jk\omega_o t} \int_{-\infty}^{\infty} R_x(t') e^{-jk\omega_o t'} dt' + \varepsilon(t, T)$$

This simplifies as:

$$T\beta_k(t) = e^{-jk\omega_o t} S_x(k\omega_o) + \varepsilon(t,T)$$

Inserting this into (2.7), we get:

$$TE\{c_k c_m^*\} = \frac{S_x(k\omega_o)}{T} \int_{-T/2}^{T/2} e^{j(m-k)\omega_o t} dt + \frac{1}{T} \int_{-T/2}^{T/2} \varepsilon(t,T) e^{jm\omega_o t} dt$$

From this we conclude that

$$TE\{c_k c_m^*\} = \begin{cases} S_x(k\omega_o) & if \quad k = m \\ 0 & if \quad k \neq m \end{cases} \tag{2.9}$$

Therefore, $E\{|c_k|^2\}$ tends to zero as $\frac{1}{T}$ for $T \to \infty$, where as the covariance $E\{c_k c_m^*\}$ tends to zero faster. In other words, the correlation coefficient ρ of the random variables tends also to zero:

$$\rho = \frac{E\{c_k c_m^*\}}{\sqrt{E\{|c_k|^2\} E\{|c_m|^2\}}} \xrightarrow[T \to \infty]{} 0$$

This means that for large T the coefficients in (2.2) are approximately uncorrelated. In order to restore the orthogonality of the coefficients, various orthogonal transforms can be used, thus losing desirable properties of the trigonometric series. The choice of a particular transform in a given application depends on the amount of reconstruction error that can be tolerated and the computational resources available. In order to retain the computational advantages of FFT and achieve decorrelation at the same time, we explore the capabilities of approximate Fourier expansion in the next session. Our goal is to present an approximate expansion of sampled signals into a Fourier series with exactly uncorrelated coefficients.

2.2 Approximate Fourier Expansion with uncorrelated coefficients

In this section, we present approximate Fourier expansion (AFE). For continuous-time non-periodic signals, an approximate Fourier expansion with theoretically uncorrelated coefficients can be expressed as[17]:

$$\hat{x}(t) = \sum_{k=-\infty}^{\infty} c_k e^{jk\omega_o t} \tag{2.10}$$

where c_k are random variables given by:

$$c_k = \int_{-\infty}^{\infty} x(t) \frac{\sin\left(\frac{\omega_o t}{2}\right)}{\pi t} e^{-jk\omega_o t} dt \tag{2.11}$$

For sampled signals, we extend the approximate Fourier expansion as[18]:

$$\hat{x}(n) = \sum_{k=-M}^{M} c_k e^{jk\omega_o n} \tag{2.12}$$

where c_k's are given by:

$$c_k = \sum_{n=-\infty}^{\infty} x(n) \frac{\sin\left(\frac{\omega_o n}{2}\right)}{\pi n} e^{-jk\omega_o n}, \quad k = 0, \pm 1, .., \pm M \tag{2.13}$$

where M is maximum number of coefficients to be computed. With signals of finite length N and $\omega_o = \frac{2\pi}{L}$, we can write discrete approximate Fourier expansion as[18]:

$$c_k = \sum_{n=0}^{N-1} x(n) \frac{\sin\left(\frac{\pi n}{L}\right)}{\pi n} e^{-j\frac{2\pi kn}{L}}, \quad k = 0, 1, \ldots, L-1 \tag{2.14}$$

where N is the length of the signal, L is a positive real number and is given by $L = \frac{2\pi}{\omega_o}$ where ω_o is resolution in frequency domain. It will be shown later that depending on the value of

ω_o, the coefficients c_k could be periodic or pseudo-periodic. The signal $x(n)$ can be reconstructed as[18]:

$$\hat{x}(n) = \sum_{k=0}^{L-1} c_k e^{j\frac{2\pi kn}{L}} \tag{2.15}$$

If the signal $x(n)$ is of finite duration $N = L$, then the pair of equations (2.14) and (2.15) can be viewed as a DFT pair of the signal $x(n)\frac{\sin\left(\frac{\pi n}{L}\right)}{\pi n}$ i.e., the signal $x(n)$ windowed by the main lobe of the sinc function. The error introduced in the reconstruction can be minimized by increasing the value of L. Alternatively, a post-reconstruction strategy can be devised to offset the effect of windowing. One way is to do an inverse windowing technique as:

$$\hat{x}(n) = \frac{1}{L}\sum_{k=0}^{L-1} c_k \frac{n\pi}{\sin\left(\frac{n\pi}{L}\right)} e^{j\frac{2\pi kn}{L}}$$

But this technique has its disadvantages. In a constrained environment where signal is transformed to a certain domain and a reduced set of coefficients is used for reconstruction, the inverse windowing will enhance channel introduced noise as well as quantization noise. Another way of reducing the windowing effect is to compute very large number L of coefficients where L is a multiple p of signal length N, and then decimate the coefficients by that multiple p. This way, the net number of coefficients is equal to N and first null of $\frac{\sin\left(\frac{n\pi}{L}\right)}{n\pi}$ falls at p times N away from the origin, reducing the windowing effect on the signal.

2.3 Properties of Approximate Fourier Expansion

In this section, we examine some important properties of this expansion[19,20]. We consider only the case of one-dimensional sampled signals.

(a) Mean value of coefficients:

$$\textit{Property}: \quad E\{c_k\} = \begin{cases} E\{x(n)\} & \textit{for} \quad k = 0 \\ 0 & \textit{otherwise} \end{cases} \tag{2.16}$$

Proof:

From equation (2.13):

$$E\{c_k\} = E\{x(n)\} \sum_{n=-\infty}^{\infty} \frac{\sin(\omega_o n/2)}{\pi n} e^{-jk\omega_o n}$$

The summation term in above equation represents the Fourier transform of $\frac{\sin\left(\frac{\omega_o n}{2}\right)}{\pi n}$ evaluated at $\omega = k\omega_o$. Since the Fourier transform of $\frac{\sin\left(\frac{\omega_o n}{2}\right)}{\pi n}$ is bandlimited between $-\frac{\omega_o}{2}$ and $\frac{\omega_o}{2}$, hence the right hand side of above equation is zero except when $k = 0$ where it has the value of 1, the property is proved.

(b) Correlation of coefficients:

Property: The coefficients of the AFE are uncorrelated.

Proof:

Consider the ideal bandpass filters of center frequency $k\omega_o$ and bandwidth ω_o as in Fig. 2.1:

$$H_k(\omega) = \begin{cases} 1 & \left(k-\frac{1}{2}\right)\omega_o < \omega < \left(k+\frac{1}{2}\right)\omega_o \\ 0 & \text{otherwise} \end{cases}$$

where $-\pi \le \omega \le \pi$ is a frequency variable. The corresponding impulse response is given by:

$$h_k(n) = e^{jk\omega_o n}\frac{\sin\left(\frac{\omega_o n}{2}\right)}{\pi n}$$

If $x(n)$ is the input to this filter, the output of kth bandpass filter will be:

$$y_k(n) = \sum_{\tau=-\infty}^{\infty} x(\tau)e^{jk\omega_o(n-\tau)}\frac{\sin\left[\frac{\omega_o(n-\tau)}{2}\right]}{\pi(n-\tau)}$$

At n = 0 we have:

$$y_k(0) = \sum_{\tau=-\infty}^{\infty} x(\tau)e^{-jk\omega_o\tau}\frac{\sin\left(\frac{\omega_o\tau}{2}\right)}{\pi\tau} = c_k \qquad (2.17)$$

Since individual filters are non-overlapping, their outputs c_k and c_m are orthogonal i.e.,

$$E\{y_k(0)y_m^*(0)\} = E\{c_k c_m^*\} = 0, \quad for \quad k \neq m \qquad (2.18)$$

Since from property *(a)*, $E\{c_k\} = 0$ except at $k = 0$, we conclude that the coefficients are also uncorrelated.

(c) Periodicity:

Property: If $\omega_o = \frac{2\pi}{L}$, and L is a rational number, then the coefficients c_k and the reconstructed signal $\hat{x}(n)$ will be periodic.

Proof:

From (2.14) it is evident that if the complex exponential is periodic, then the coefficients will be periodic in k. If $L = \frac{P}{Q}$ where P, Q are integers and L is a rational number, then $e^{-j2\pi\frac{Q}{P}kn}$ will be periodic with period P. From (2.15) it can be noticed that the reconstructed signal will be also periodic with the same period. Under these conditions, the upper limit of the summation in (2.15) can be P. In the special case where L is an integer (Q = 1), then the period will be L. It should also be noted that when L is an irrational number, then there will be a "pseudo-periodicity" in the coefficients with period $P = \text{int}\{L\}$, i.e., the coefficients within a pseudo-period P will not be equal, but approximately similar. From this it can be concluded that an integer value of L will always result in a computation of less number of coefficients.

(d) Mean value of reconstructed signal:

$$\textit{Property}: \quad E\{\hat{x}(n)\} = E\{x(n)\} \tag{2.19}$$

Proof:

Using equation (2.15):

$$E\{\hat{x}(n)\} = E\left[\sum_{k=0}^{L-1} c_k e^{j\frac{2\pi kn}{L}}\right]$$

We know from property (*a*):

$$E\{c_k\} = \begin{cases} E\{x(n)\} & for \quad k = 0 \\ 0 & otherwise \end{cases}$$

At k=0 and using this result, we have in mean-square sense:

$$E\{\hat{x}(n)\} \quad = \quad E\{c_o\} \quad = \quad E\{x(n)\}$$

This equation suggests that reconstructed signal $\hat{x}(n)$ gives mean square approximation to $x(n)$.

(e) Mean square value of coefficients:

$$\textit{Property:}\quad E\{|c_k|^2\} = \frac{1}{2\pi}\int_{(k-1/2)\omega_o}^{(k+1/2)\omega_o} S_x(\omega)d\omega \tag{2.20}$$

Proof:

Consider the ideal bandpass filters of center frequency $k\omega_o$ and bandwidth ω_o as in Fig. 2.1:

$$H_k(\omega) = \begin{cases} 1 & \left(k-\frac{1}{2}\right)\omega_o < \omega < \left(k+\frac{1}{2}\right)\omega_o \\ 0 & \textit{otherwise} \end{cases}$$

where $-\pi \le \omega \le \pi$ is a frequency variable.

The power spectrum of output of the sub-filter k is given by:

$$S_y(\omega) = S_x(\omega) \quad |H_k(\omega)|^2$$

Taking inverse Fourier transform of both sides, we get:

$$E\{|y_k(n)|^2\} = \frac{1}{2\pi}\int_{-\pi}^{\pi} S_x(\omega) \quad |H_k(\omega)|^2 \quad e^{j\omega n}d\omega$$

Using the limits of $H_k(\omega)$, we get, at n=0:

$$E\{|y_k(0)|^2\} = \frac{1}{2\pi}\int_{(k-1/2)\omega_o}^{(k+1/2)\omega_o} S_x(\omega) \quad d\omega$$

Using result in equation (2.17):

$$E\{|c_k|^2\} = \frac{1}{2\pi} \int_{(k-1/2)\omega_o}^{(k+1/2)\omega_o} S_x(\omega) \quad d\omega$$

which is area under kth pulse. If ω_o is very small so that $S_x(\omega)$ is constant S_x in that interval then:

$$E\{|c_k|^2\} = \frac{S_x}{2\pi} * \omega_o = \frac{S_x}{L}$$

which means that we are sampling the spectrum of original signal at sufficient number L of frequency points with area of each impulse as $\frac{S_x}{L}$.

(f) Mean square value of reconstructed signal:

Property: $E\{|\hat{x}(n)|^2\} = E\{|x(n)|^2\}$ (2.21)

Proof:

From equation (2.15):

$$E\{|\hat{x}(n)|^2\} = E\left\{\sum_{k=0}^{L-1} c_k e^{jk\omega_o n} \sum_{m=0}^{L-1} c_m e^{-jm\omega_o n}\right\}$$

Using $\omega_o = \frac{2\pi}{L}$ with L as an integer, therefore:

$$E\{|\hat{x}(n)|^2\} = E\left\{\sum_{k=0}^{L-1}\sum_{m=0}^{L-1} c_k c_m e^{j(k-m)\omega_o n}\right\} = \sum_{k=0}^{L-1}\sum_{m=0}^{L-1} E\{c_k c_m\} E\left\{e^{j\frac{2\pi(k-m)n}{L}}\right\}$$

$$E\{|\hat{x}(n)|^2\} = \sum_{k=0}^{L-1}\sum_{m=0}^{L-1} E\{c_k c_m\} * \frac{1}{N}\sum_{n=0}^{N-1} e^{j\frac{2\pi(k-m)n}{L}}$$

Since $e^{j\frac{2\pi kn}{L}}$ are orthogonal over period L for $k \neq m$, therefore we have at $k = m$:

$$E\{|\hat{x}(n)|^2\} = \sum_{k=0}^{L-1} E\{|c_k|^2\}$$

Using property (*e*), we get:

$$E\{|\hat{x}(n)|^2\} = \sum_{k=0}^{L-1} \frac{1}{2\pi} \int_{(k-1/2)\omega_o}^{(k+1/2)\omega_o} S_x(\omega) \quad d\omega \tag{2.22}$$

If ω_o is very very small so that $L = \frac{2\pi}{\omega_o}$ is sufficiently large for minimum reconstruction error and $S_x(\omega)$ is constant in that interval ω_o, then the above equation becomes:

$$E\{|\hat{x}(n)|^2\} = \frac{1}{2\pi} \int_{-\pi}^{\pi} S_x(\omega) \quad d\omega = \frac{1}{2\pi} \int_{-\pi}^{\pi} S_x(\omega) \quad d\omega$$

$$E\{|\hat{x}(n)|^2\} = E\{|x(n)|^2\}$$

g) Spectrum of reconstructed signal:

$$\textit{Property}: \quad S_{\hat{x}}(\omega) = N \sum_{k=0}^{L-1} E\{|c_k|^2\}\delta(\omega - k\omega_o) \tag{2.23}$$

Proof:

Assume that signal is of finite length N, then applying Fourier transform on equation (2.15):

$$\hat{X}(\omega) = \sum_{n=0}^{N-1} \hat{x}(n) e^{-j\omega n}$$

$$\hat{X}(\omega) = \sum_{n=0}^{N-1} \left\{ \sum_{k=0}^{L-1} c_k e^{jk\omega_o n} \right\} e^{-j\omega n}$$

$$\hat{X}(\omega) = \sum_{k=0}^{L-1} c_k \left\{ \sum_{n=0}^{N-1} e^{-j(\omega - k\omega_o)n} \right\}$$

The term in brackets on right hand side evaluates to

$$\sum_{n=0}^{N-1} e^{-j(\omega - k\omega_o)n} = \begin{cases} N & \omega = k\omega_o \\ 0 & \textit{otherwise} \end{cases}$$

Therefore:

$$S_{\hat{x}}(\omega) = E\{|\hat{X}(\omega)|^2\} = N \sum_{k=0}^{L-1} E\{|c_k|^2\}\delta(\omega - k\omega_o)$$

This means that the Fourier transform of the recovered signal is a series of impulses with resolution of ω_o. The area under each impulse equals the area under $S_x(\omega)$ in an interval of length ω_o centered at $\omega = k\omega_o$. For an arbitrary lowpass signal, the $S_{\hat{x}}(\omega)$ is given in Fig. 2.2.

(h) Autocorrelation of reconstructed signal:

$$\textit{Property}: \quad R_{\hat{x}}(n) = R_x(n) \tag{2.24}$$

Proof:

$$R_{\hat{x}}(\tau) = E\{\hat{x}(n+\tau)\hat{x}^*(n)\} = E\left\{\sum_{k=0}^{L-1} c_k e^{jk\omega_o(n+\tau)} \sum_{m=0}^{L-1} c_m e^{-jm\omega_o n}\right\}$$

Since $E\{c_k c_m\} = 0$, except at k=m. Therefore:

$$R_{\hat{x}}(\tau) = \sum_{k=0}^{L-1} E\{|c_k|^2\} \quad e^{jk\omega_o\tau}$$

Using property (*e*), we get:

$$R_{\hat{x}}(\tau) = \sum_{k=0}^{L-1}\left[\frac{1}{2\pi}\int_{(k-1/2)\omega_o}^{(k+1/2)\omega_o} S_x(\omega)d\omega\right] \quad e^{jk\omega_o\tau}$$

As $\omega_o \to 0$, we have:

$$R_{\hat{x}}(\tau) = \frac{1}{2\pi}\int_{-\pi}^{\pi} S_x(\omega)e^{jk\omega_o\tau}d\omega = R_x(\tau)$$

Since the expected value of the reconstructed signal (property '*d*') is a constant and the autocorrelation of $\hat{x}(n)$ does not depend on time n, hence the recovered signal is wide-sense stationary.

(i) Trigonometric properties:

Properties: The approximate Fourier expansion has all properties of a trigonometric series expansion, namely:

linearity, time shift, scaling, translation, conjugate symmetry, rotation, separability.

Proof:

If we define

$$x'(n) = x(n)\frac{\sin\left(\frac{\omega_o n}{2}\right)}{\pi n}$$

and write $\omega_o = \frac{2\pi}{L}$, where L is an integer then:

$$\hat{x}(n) = \sum_{k=0}^{L-1} c_k e^{j\frac{2\pi kn}{L}}$$

where c_k's are given by:

$$c_k = \sum_{n=-\infty}^{\infty} x'(n) e^{-j\frac{2\pi kn}{L}}$$

These equations are similar to discrete Fourier transform, hence they also possess all trigonometric series properties.

2.4 Error Analysis

In this section, we will compute the mean square error between original and reconstructed signal. The main objective here is to evaluate an upper bound on ω_o so that error does not exceed certain percentage of the average power of $x(n)$. We define the mean square error as:

$$e_{ms} = E\{|x(n)-\hat{x}(n)|^2\}$$

$$e_{ms} = 2E\{|\hat{x}(n)|^2\}-2E\{|x(n)\hat{x}(n)^*|\} \quad (2.25)$$

Here, We have used the property (*f*) that $E\{|x(n)|^2\}=E\{|\hat{x}(n)|^2\}$. Using $c_k = y_k(0)$ (output of sub-filter *k*) as shown in equation (2.17), we get:

$$E\{x(n)c_k^*\} = E\{x(n)y_k^*(0)\} = R_{xy_k}(n)$$

But cross-power-spectrum of $x(n)$ and $y_k(n)$ equals $S_x(\omega)H_k^*(\omega)$; therefore:

$$E\{x(n)c_k^*\}=\frac{1}{2\pi}\int_{\pi}^{\pi} S_x(\omega)H_k^*(\omega)e^{j\omega n}d\omega=\frac{1}{2\pi}\int_{(k-1/2)\omega_o}^{(k+1/2)\omega_o} S_x(\omega)e^{j\omega n}d\omega$$

Summing along all coefficients, we get:

$$\sum_{k=0}^{L-1} E\{x(n)c_k^*\}e^{-jk\omega_o n}=\frac{1}{2\pi}\sum_{k=0}^{L-1}\int_{(k-1/2)\omega_o}^{(k+1/2)\omega_o} S_x(\omega)e^{j(\omega-k\omega_o)n}d\omega$$

$$E\{x(n)\hat{x}^*(n)\}=\frac{1}{2\pi}\sum_{k=0}^{L-1}\int_{(k-1/2)\omega_o}^{(k+1/2)\omega_o} S_x(\omega)e^{j(\omega-k\omega_o)n}d\omega=\frac{1}{2\pi}\sum_{k=0}^{L-1}\int_{(k-1/2)\omega_o}^{(k+1/2)\omega_o} S_x(\omega)\left[\cos(\omega-k\omega_o)n+j\sin(\omega-k\omega_o)n\right]d\omega$$

Since $S_x(\omega)$ is an even function therefore second term in above equation equates to zero:

$$E\{x(n)\hat{x}^*(n)\} = \frac{1}{2\pi}\sum_{k=0}^{L-1}\int_{(k-1/2)\omega_o}^{(k+1/2)\omega_o} S_x(\omega) \quad \cos[(\omega - k\omega_o)n] \quad d\omega$$

Putting this value and the result from equation (2.22) in equation (2.25), we get:

$$e_{ms} = \frac{1}{\pi} \sum_{k=0}^{L-1}\int_{(k-1/2)\omega_o}^{(k+1/2)\omega_o} S_x(\omega) \quad [1 - \cos(\omega - k\omega_o)n] \quad d\omega \tag{2.26}$$

For an arbitrary low pass signal, this equation is plotted in Fig. 2.3*a*. The second part of this equation depends on n and is generated by $E\{|x(n)\hat{x}^*(n)|\}$. This shows that the $x(n)$ and $\hat{x}(n)$ are individually but not jointly wide-sense stationary. If they were, the mean-square error e_{ms} would be independent of time.

The above is a worst case estimate assuming that $S_x(\omega)$ is concentrated at the end points of each integration interval *i.e* from $(k-1/2)\omega_o$ to $(k+1/2)\omega_o$. If $S_x(\omega)$ does not vary appreciably in these intervals, then equation (2.26) can be modified by replacing $S_x(\omega)$ by a constant in each integration interval as:

$$e_{ms} = \frac{1}{\pi}\sum_{k=0}^{L-1} S_x(\omega)\left[\omega_o - \frac{\sin(\omega_o n/2)}{n} - \frac{\sin(\omega_o n/2)}{n}\right] = \frac{1}{\pi}\sum_{k=0}^{L-1} S_x(\omega) \quad \omega_o\left[1 - \frac{\sin(\omega_o n/2)}{\omega_o n/2}\right]$$

$$e_{ms} = 2\left[1 - \frac{\sin(\omega_o n/2)}{\omega_o n/2}\right] \quad \frac{1}{2\pi}\sum_{k=0}^{L-1} \omega_o S_x(\omega)$$

This can be simplified as:

$$e_{ms} \approx 2 \quad E\{|x(n)|^2\} \quad \left[1 - \frac{\sin\left(\frac{\omega_o n}{2}\right)}{\frac{\omega_o n}{2}}\right] \tag{2.27}$$

This means that in the limit as ω_o tends to zero, mean square error approaches zero in mean-square sense. We can also deduce from equation (2.27) that in order for mean square error not to exceed certain percentage of average power of $x(n)$, the first null of sinc function in equation (2.27) shall fall very far away from origin.

Upper bound on error:

In equation (2.15) if $\omega_o n < \pi$ for every n in (0,N-1) where N is the length of the signal, then from equation (2.26) we have:

$$1-\cos(\omega-k\omega_o)n \quad = \quad 2 \quad \sin^2\frac{(\omega-k\omega_o)n}{2} \quad < \quad 2 \quad \sin^2\left(\frac{\omega_o n}{4}\right)$$

for every ω such that $|\omega-k\omega_o| < \frac{\omega_o}{2}$. Therefore,

$$e \le \frac{2}{\pi}\sin^2\left(\frac{\omega_o n}{4}\right)\int_{-\pi}^{\pi} S_x(\omega)d\omega$$

Rearranging the right hand side of the above equation, we get:

$$e \le 4\sin^2\left(\frac{\omega_o n}{4}\right) \quad \frac{1}{2\pi}\int_{-\pi}^{\pi} S_x(\omega)d\omega$$

$$e \le 4\sin^2\left(\frac{\omega_o n}{4}\right) \quad E\{|x(n)|^2\} \tag{2.28}$$

This equation means that in order for mean square error not to exceed certain percentage of the average power of $x(n)$, ω_o should be chosen such that

$$4\sin^2(\omega_o N/4) \quad \ll \quad 1 \tag{2.29}$$

This equation is plotted in Fig. 2.3*b* for various value of L, which shows that relatively larger values of L yield lower mean square error in the reconstructed signal.

2.5 Approximate Cosine Expansion

In this section, we develop an approximate cosine expansion (ACE)[21] from an approximate Fourier expansion (AFE) and show that for the same L it introduces less reconstruction error than discrete approximate Fourier expansion (AFE) with the advantage that the coefficients are real.

Consider Fig. 2.4(*a*) and Fig. 2.4(*b*), which represent sampled data, and the reconstructed signal after applying an AFE. It should be noted that L used was an integer and sufficiently large for minimum reconstruction error. Since the AFE coefficients and the reconstructed signal are periodic with period L, Fig. 2.4(*b*) contains severe discontinuities between the segments and these result in spurious spectral components. This discontinuity can be removed by making the data to be transformed symmetric, i.e by folding it about the vertical axis (along the origin) as shown in Fig. 2.4(*c*), and then overlapping the two halves by one element. Folding the data has given us an even function to transform. We now apply an AFE of length $2L$ to the data of length $2N$. Note that the axis of symmetry in Fig. 2.4(*c*) lies at the point $n = -\frac{1}{2}$ i.e., 1/2 point to the left of the signal at the origin. Therefore, applying an AFE to the signal in Fig. 2.4(*c*), we get:

$$c_k = \sum_{n=-N}^{N-1} x(n) \frac{\sin\left(\frac{n\pi}{2L}\right)}{n\pi} e^{-j\frac{2\pi k\left(n+\frac{1}{2}\right)}{2L}} \tag{2.30}$$

Since $x(n)$ is real and even, therefore:

$$c_k = 2\sum_{n=0}^{N-1} x(n)\frac{\sin\left(\frac{n\pi}{2L}\right)}{n\pi}\cos\left[\frac{\pi k(2n+1)}{2L}\right], \quad k = 0, 1, \ldots, L-1 \tag{2.31}$$

The $x(n)$ is reconstructed using equation (2.15) as:

$$\hat{x}(n) = \sum_{k=0}^{L-1} c_k e^{j\frac{\pi k(2n+1)}{2L}}$$

Since c_k's are real and even as they are generated by symmetric extension of input signal, therefore:

$$\hat{x}(n) = 2\sum_{k=0}^{L-1} c_k \cos\frac{\pi k(2n+1)}{2L} \tag{2.32}$$

Letting $L_1 = 2L$, then equation (2.31) can be rewritten as:

$$c_k = 2 \quad Re\left[\sum_{n=0}^{N-1} x(n)\frac{\sin\left(\frac{n\pi}{L_1}\right)}{n\pi} e^{-j\frac{2\pi kn}{L_1}} \quad e^{-j\frac{\pi k}{L_1}}\right] \tag{2.33}$$

The term in the brackets is similar to c_k in equation (2.14) (with L replaced by L_1) multiplied by an exponential term. Since $L_1 = 2L$,therefore$\omega_o = \frac{2\pi}{L_1} = \frac{\pi}{L}$. This means that first null of $\sin\left(\frac{n\pi}{L_1}\right)$will fall at $2L$ instead of at L. In other words, the error introduced in the reconstructed signal will be less than the error due to applying AFE on the signal.

2.6 Simulations

In this section, we will test and verify the results obtained in section 2.1 through 2.5. The performance of the expansions will be evaluated using objective fidelity criterion. An objective fidelity criterion is the mean square signal to noise ratio (SNR_{ms}). Here we define mean square signal to noise ratio as:

$$SNR_{ms} = \frac{\sum_{i=0}^{N-1}\sum_{j=0}^{N-1}(\hat{x}_{ij})^2}{\sum_{i=0}^{N-1}\sum_{j=0}^{N-1}(x_{i,j}-\hat{x}_{i,j})^2} \tag{2.33}$$

Since the performance of these expansions depends on the choice of $\omega_o = \frac{2\pi}{L}$, these expansions were applied to a length (N=128) of a speech signal and "Lena" image, and SNR_{ms} was computed for various values of L. Results are shown in Figs. 2.6 and 2.7. Fig. 2.5 displays a segment of original speech signal under test, whereas Figs. 2.6*a*, 2.6*b* and 2.6*c*, 2.6*d* show the reconstructed speech signal using AFE and ACE respectively for two different values of L. Similarly, Fig. 7*a* displays original "Lena" image of size 256x256, where as Fig. 7*b*, Fig. 7*c* and Fig. 7*d*, Fig. 7*e* display reconstructed "Lena" image using AFE and ACE respectively for two different values of L. It is obvious from Figs. 2.6 and 2.7 that smaller values of ω_o produce closer approximations. This is expected since smaller values of ω_o result in finer sampling resolution, where as larger values of ω_o produce a coarse resolution resulting in a large error. Fig. 2.8 shows SNR_{ms} of the reconstructed speech signal when L varies from low to high in AFE reconstruction of the speech signal. It is clear from this Fig. that relatively larger values of L yield higher SNR_{ms}.

In order to compare the performance of ACE with discrete cosine transform (DCT), we tested the cross correlation and variance of DCT and ACE coefficients by applying ACE

and DCT on blocks of a speech signal. We took blocks of 128 samples of speech signal and applied DCT and ACE with L=128 on each block. In order to compute cross correlation and variance of coefficients, we computed cross correlation of each coefficient with other coefficients in a block and the result was averaged across all of the blocks in a speech signal. The result in shown in Fig. 2.9 as an intensity image. It is obvious from the Fig. 2.9 that intensity of the image off the diagonal in Fig. 2.9*b* is very low as compared to Fig. 2.9*a* which demonstrates that ACE gives relatively better decorrelation than DCT. The variance of the coefficients can be obtained by plotting diagonal elements of the intensity image. This result is shown in Fig. 2.10. It is obvious from Fig. 2.10 that variance of ACE coefficients is less than that of the DCT coefficients.

From all these results, it can be claimed that ACE can be applied to 1-D signals for coding applications. We will explore this further in the next chapter.

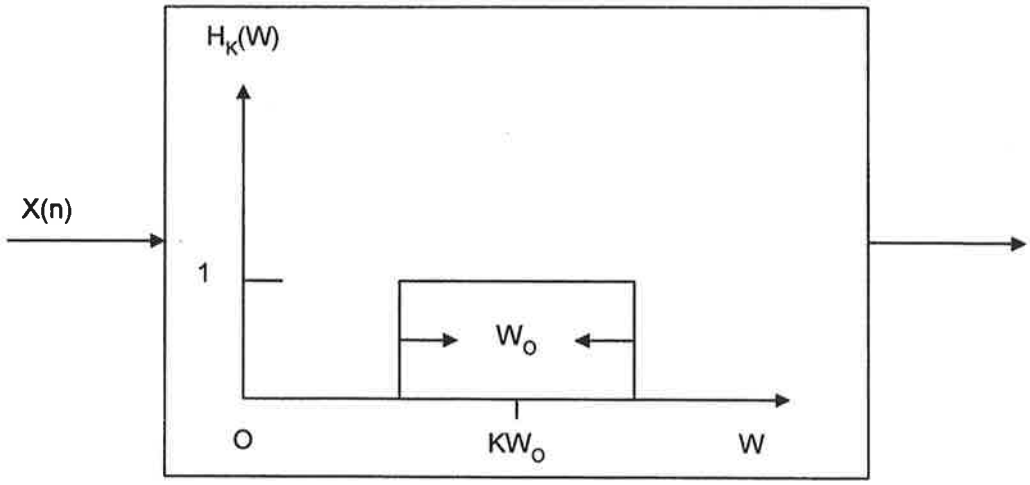

Fig. 2.1. Ideal bandpass filter

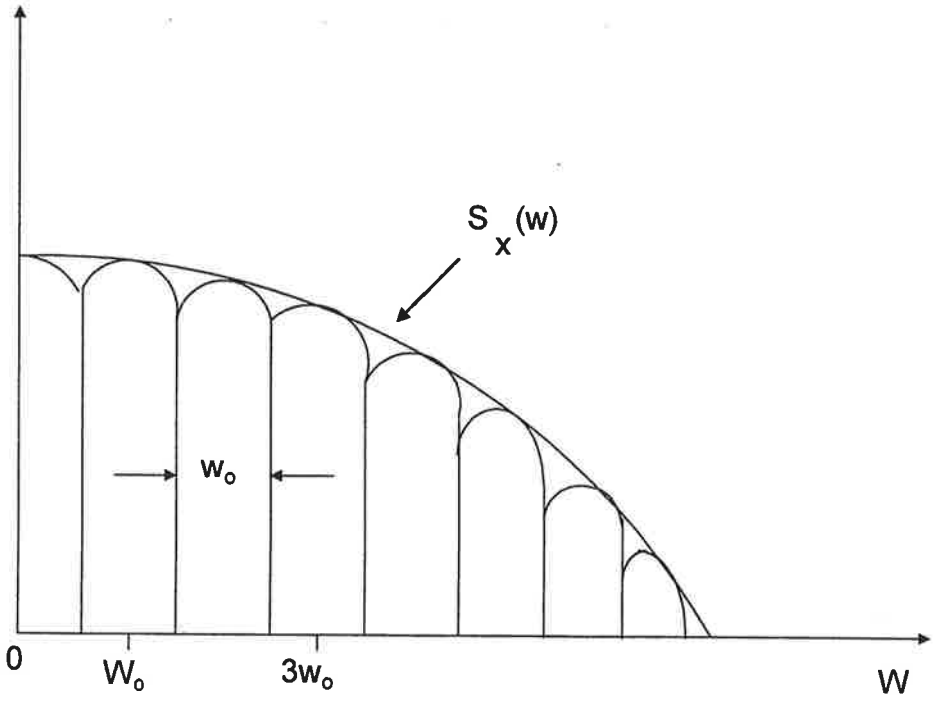

Fig. 2.2 Spectrum of reconstructed signal

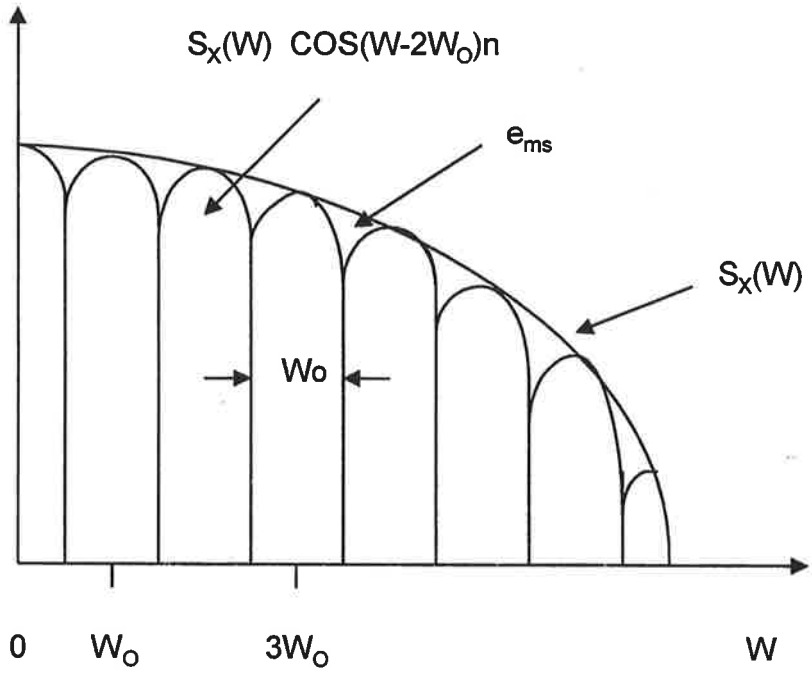

Fig. 2.3a. Mean square error of an arbitrary lowpass signal

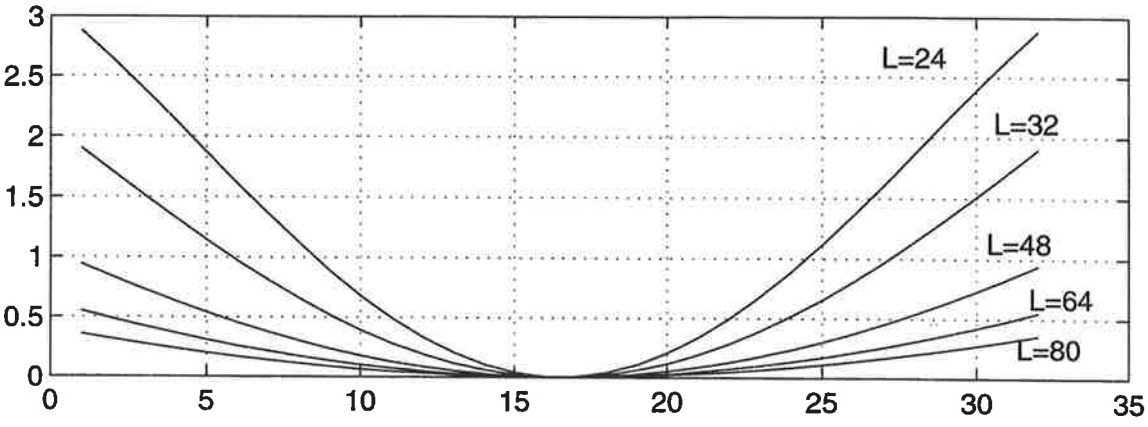

Fig. 2.3*b* Upper bound on mean square error for various value of L

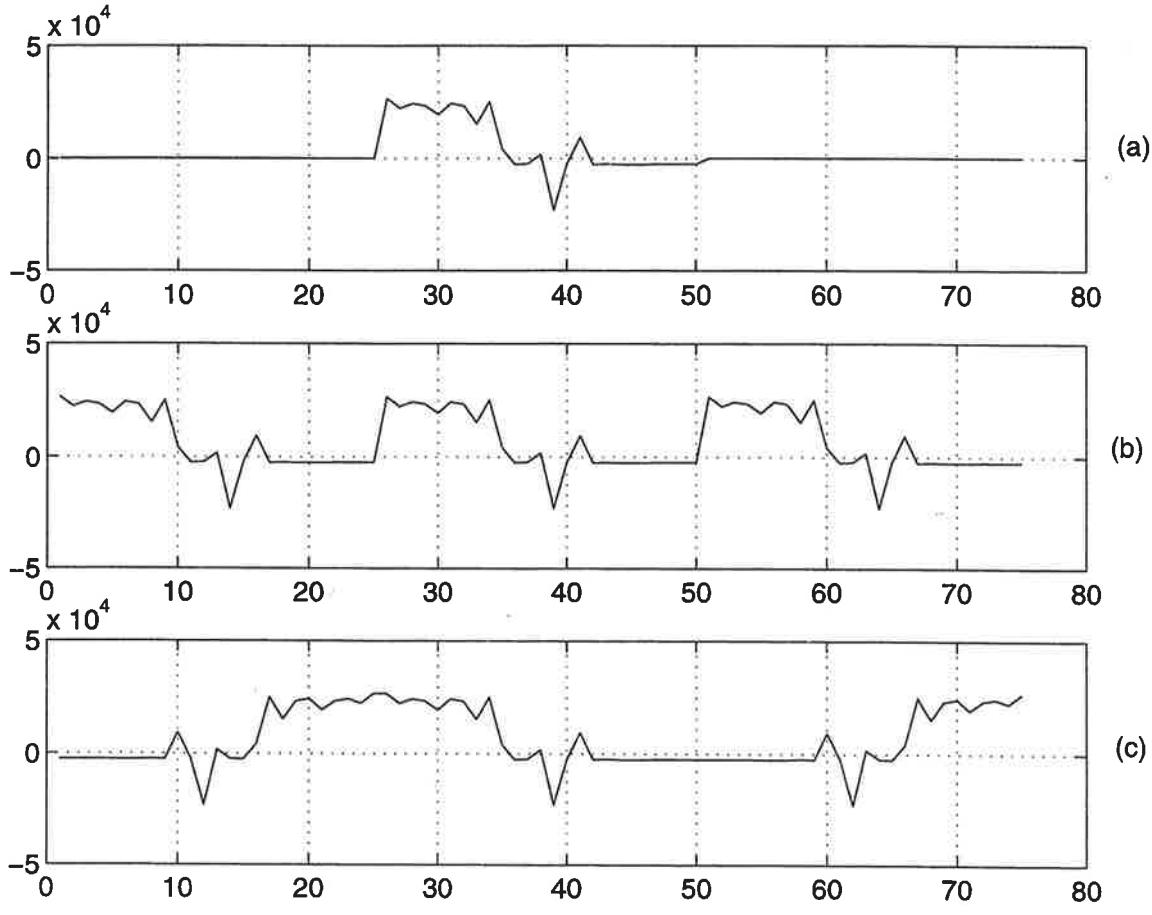

Fig. 2.4 (*a*) Signal length for analysis, (*b*) Data domain equivalent of AFE coefficients, (*c*) Data folded to eliminate discontinuity

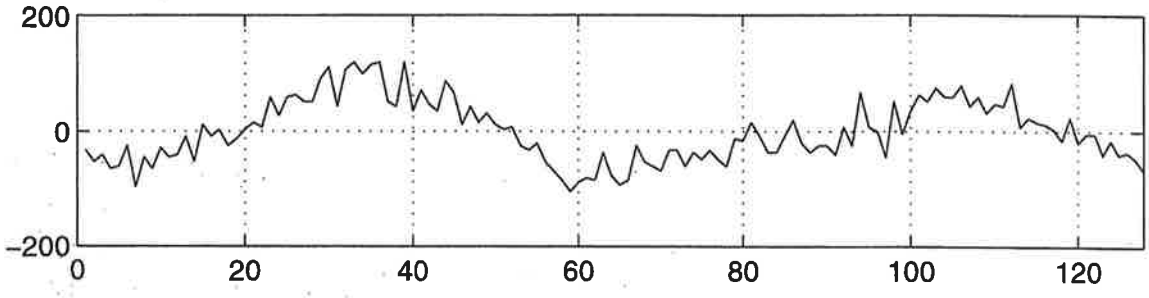

Fig. 2.5 A segment of original speech signal

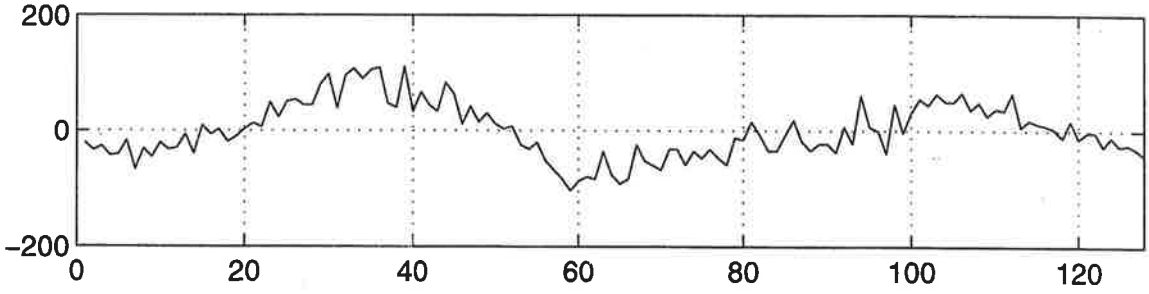

Fig. 2.6*a* Speech signal reconstructed with L=128

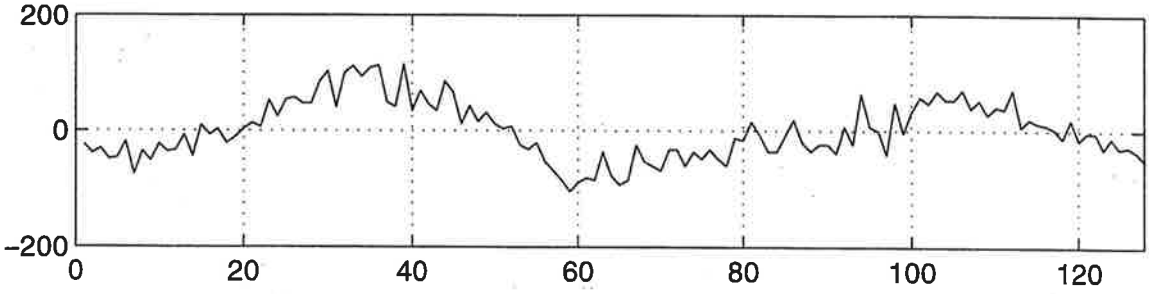

Fig. 2.6*b* Speech signal reconstructed with L=150

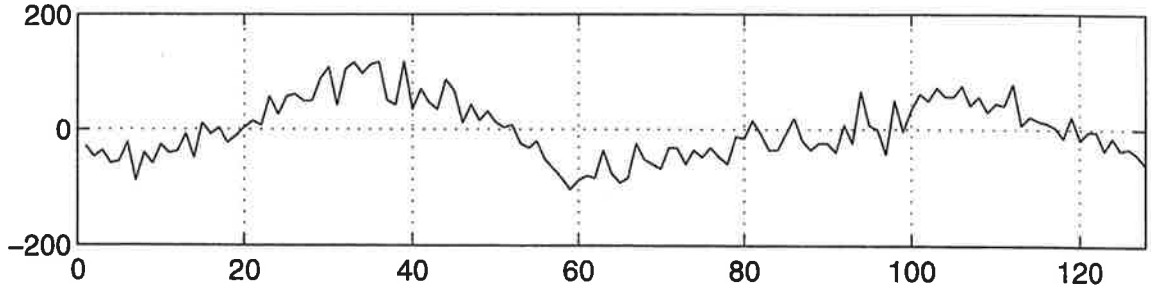

Fig. 2.6*c* Speech signal reconstructed wit L=128

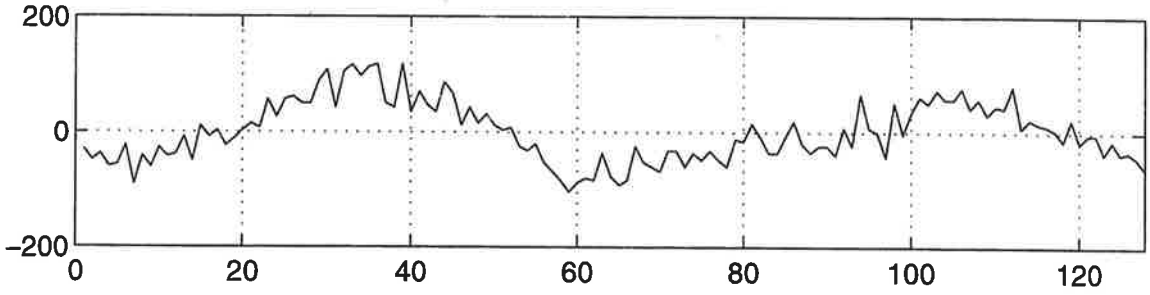

Fig. 2.6*d* Speech signal reconstructed with L=150

Fig. 2.7*a* Original "Lena" image, N=256x256

Fig. 2.7*b* "Lena" image reconstructed with L=256, using AFE

Fig. 2.7*c* "Lena" image reconstructed with L=280, using AFE

Fig. 2.7*d* "Lena" image reconstructed with L=256, using ACE

Fig. 2.7*e* "Lena" image reconstructed with L=280, using ACE

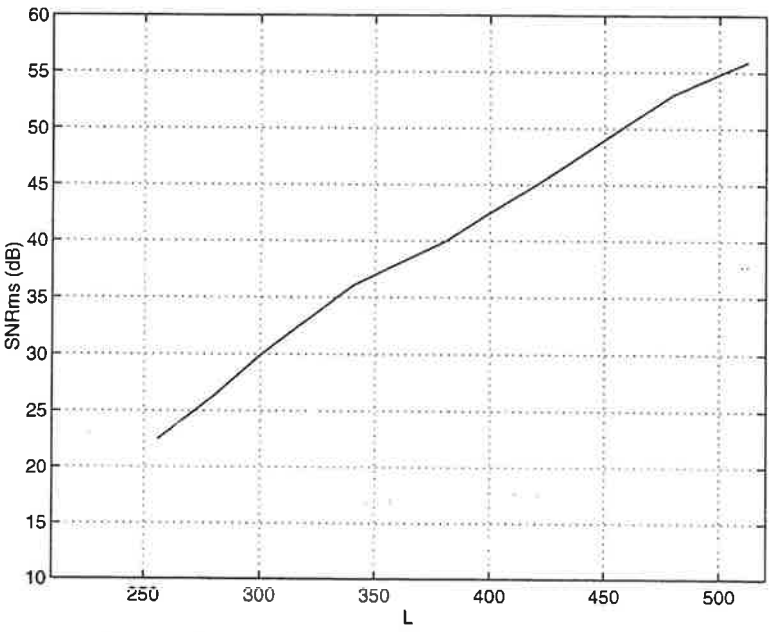

Fig. 2.8 SNR_{ms} vs. L

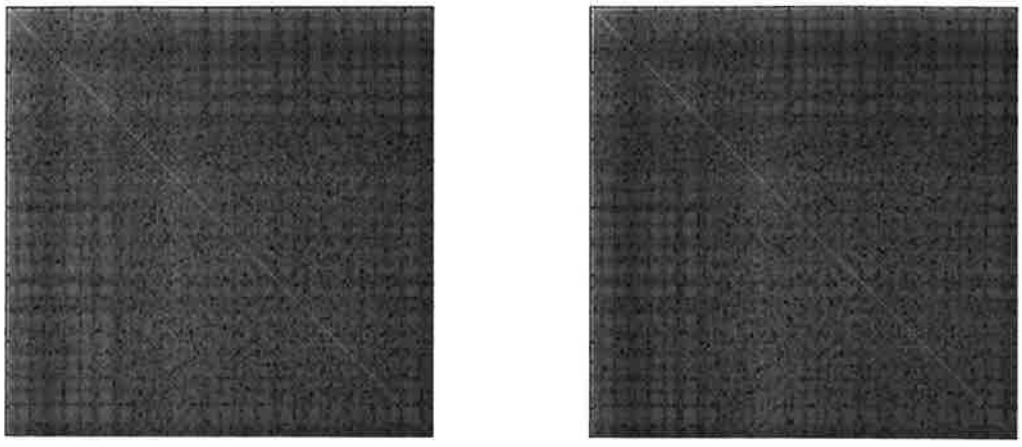

Fig. 2.9 Cross-correlation of DCT (left Fig.) and ACE (right Fig.) coefficients

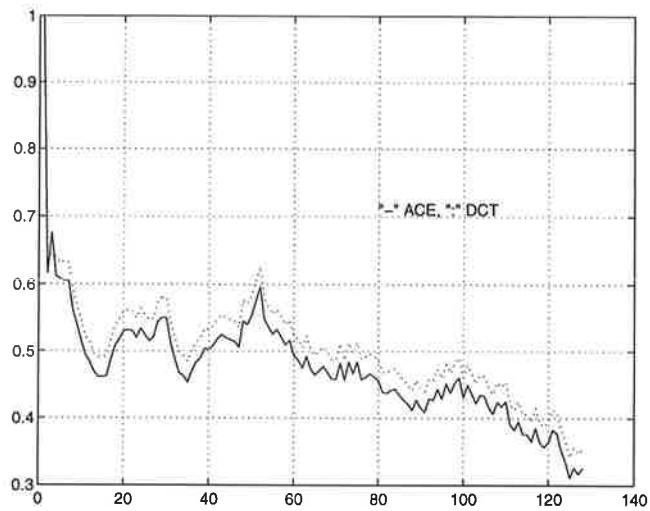

Fig. 2.10 Variance of DCT/ACE coefficients

3 . MULTIRESOLUTION SIGNAL DECOMPOSITION USING THE APPROXIMATE FOURIER EXPANSION

3.1 Introduction

Digital data nowadays, in contrast to a decade or so ago, is available in a wide variety of resolutions, and a spectrum of applications exists in which there is requirement to (re)generate basically the same data at different levels of definition. Thus it may be required (notwithstanding the different aspect ratio) to reproduce high definition television images on standard definition displays, transmit segments of a television or video conferencing image at a reduced resolution over a video-telephone system, or an image reproduced initially at low resolution may require that resolution to be gracefully improved with time in an image browsing facility. In the latter case, such progressive transmission reproduces a low resolution image quickly, after which detail can be built through time as the viewer desires, and coding schemes can be arranged to process an image broken down into a low detail version together with a signal representing the otherwise lost definition, the two components being added during the reconstruction stage at the receiver. There is a general interest, therefore, in developing algorithms which compute versions of the same picture at different resolutions, together with an additional detail signal which represents what is lost in going from one level of resolution to another, lower, one and which, when added to the latter, allows reconstruction of the former. The present high degree of interest in wavelet decomposition of signals in one or more dimensions into subsets at various levels of resolution has naturally led to applications in the areas of signal coding. The basic idea is to divide the signal frequency band into a set of uncorrelated frequency bands by filtering and then to encode each

of these subbands using a bit allocation rationale matched to the signal energy in that subband. The subband coder achieves energy compaction by filtering serial data whereas transform coding utilizes block transformation. If the subbands have little spill over from adjacent bands (as would be case if the subband filters have sharp cutoffs), the quantization noise in a given band is limited largely to that band. This permits separate, band-by-band allocation of bits, and controls of this noise in each band.

The purpose of transform coding is to decompose a set of correlated signal samples into a set of uncorrelated spectral coefficients with energy concentrated in as few coefficients as possible. The uneven distribution of signal energy in frequency domain has made signal decomposition an important practical problem. The recent activity in signal decomposition is driven by signal processing and coding applications. More recently, the wavelet transform with the capability for variable time-frequency resolution has gained a considerable attention as an elegant multiresolution signal processing tool. The basic concept is to divide the signal spectrum into its subbands and then treat those subbands individually for the purpose of signal representation or coding. This technique has two desirable features. First, monitoring of signal energy within subbands is possible and then the subbands can be ranked and processed independently. Second, the subband decomposition leads to multiresolution signal decomposition of the signal spectrum. The signal can thus be represented at each resolution. Therefore, the basic objective in signal analysis is to devise a transformation that represents signal features simultaneously in time and frequency.

Discrete approximate trigonometric expansions were, in last chapter, analyzed as signal transformation tool for encoding applications. These approximate trigonometric expansions have a user-defined parameter which can be used for making the transformation

a signal decomposition tool. In this chapter, we explore the capability of an approximate Fourier expansion (AFE) as a decomposition tool for 1-D signals and images. Furthermore, the decomposed signals will also be represented by an approximate cosine expansion (ACE) which is actually an approximate Fourier expansion (AFE) of a symmetric extension of the signal. Thus approximate Fourier expansion can be used as a single tool for signal decomposition as well as representation technique as compared to subband decomposition combined with single or mixed transforms.

This chapter is organized as follows: In section 3.2, we briefly discuss multiresolution decomposition of the signal. In section 3.3, we explore the capability of the approximate Fourier expansion as a signal decomposition tool. Specifically, we present system interpretation of an approximate Fourier expansion (AFE) using generalized harmonic analysis. In section 3.4, we present determination of transformation efficiency using first order Markov process. Section 3.5 presents simulation results carried out on 1-D signals and images.

3.2 Multiresolution Signal Decomposition

Many of the developments preceding wavelet analysis came in a field generally called *multiresolution analysis*. These developments were intended to combat the limitations of the Fourier transform. Filter bank theory used in wavelet analysis offers a convenient means of representing signals composed of oscillatory components, such as musical notes and tone bursts. These components include several (or many) cycles of the oscillation within their duration. In image analysis, however, the localized components of interest often are not truly oscillatory, in that they include only one cycle or even just part of a cycle. Examples

include lines, edges, and spots. The objects in an image are observed to occur at different scales. An edge, for example, can be either a sharp transition from black to white or one that occurs gradually over a considerable distance. In general, a multiresolution approach to image representation or analysis seeks to exploit this idea.

Cartography illustrates the approach. Maps are commonly drawn at different scales. The scale of a map is the ratio of the size of an actual territory to that of its representation on the map. At large scales, as on a globe, major features such as continents, oceans, country boundries are visible, while details become visible and larger features are lost. Thus, to be able to navigate to a point at a distant location, one needs a set of maps drawn at different scales.

Wavelet transforms have developed along these multiresolution lines. As with time-frequency analysis, a signal is represented in a two-dimensional space, but here the vertical axis is scale rather than frequency. Scaling is achieved by dilating and contracting the basic wavelet to form a set of basis functions. The ability of the wavelet transform to operate at various scales (resolution levels) has afforded an efficient technique, which is closely related to Burt and Adelson's[22] work, for multiresolution analysis and which can, in fact, be viewed as an implementation of a particular kind of subband decomposition. The design of the Laplacian pyramid[22] provided the inspiration that later led to the discrete wavelet transform. As a further background leading to the discrete wavelet transform, a time-frequency technique called *subband coding*, originally developed for compact coding of digitized audio signals, seeks to decompose a signal (or an image) into narrow-band (bandpass filtered) components and represent these, without redundancy, in such a way that it is possible to reconstruct the original signal without error[23-25]. Mallat[26] defined a discrete wavelet

transform algorithm, which applies two-band subband coding in an iterative fashion and builds the wavelet transform from bottom up, that is, computing small-scale coefficients first.

At the first stage, subband coding is applied on the signal. After the first step of subband coding, the lower subband signal is once again subjected to halfband subband coding. This leaves us with the N/2-point upper halfband signal and two N/4-point subband signals. The process is continued, at each step retaining the upper halfband signal and further encoding the lower halfband signal, until a one-point low band signal is obtained. The transform coefficients are then the low band point and the collection of subband coded upper halfband signals. This is shown in Fig. 3.1. The impulse response doubles in scale at each iteration. Thus, we have an orthonormal wavelet transform. The subband coding, which is basically a time-frequency transform technique, has been employed to define a time-scale wavelet transform. This algorithm is sometimes referred to as the *fast wavelet transform* (FWT), or Mallat's herringbone algorithm, due to the appearance of the diagram in Fig. 3.1. The inverse transform is obtained by reversing the process, as shown in Fig. 3.2.

3.3 Signal Decomposition using the Approximate Fourier Expansion

In this section, we explore the capability of the approximate trigonometric expansions as a signal decomposition as well as representation tool. We also present a system interpretation of the approximate Fourier expansion (AFE) using the *Generalized harmonic* analysis. Consider a stochastic process $x(t)$ with generalized transform $G(\omega)$, where $G(\omega)$ of a stochastic process $x(t)$ is defined by[17]:

$$G(\omega_1) - G(\omega_2) = \int_{-\infty}^{\infty} \frac{e^{-j\omega_1 t} - e^{-j\omega_2 t}}{-jt} x(t)dt \tag{3.1}$$

Where $G(\omega)$ is determined from above equation within a constant. The above equation can further be simplified as:

$$G(\omega_1) - G(\omega_2) = \int_{-\infty}^{\infty} x(t) \int_{\omega_2}^{\omega_1} e^{-j\omega t} d\omega \quad dt = \int_{\omega_2}^{\omega_1} \int_{-\infty}^{\infty} x(t) e^{-j\omega t} dt d\omega$$

If $x(t)$ has a Fourier transform $X(\omega)$, then this means:

$$G(\omega_1) - G(\omega_2) = \int_{\omega_2}^{\omega_1} X(\omega) d\omega \quad \Rightarrow \quad X(\omega) = \frac{dG(\omega)}{d\omega} \tag{3.2}$$

Further if $\omega_1 = \omega + \varepsilon, \omega_2 = \omega - \varepsilon$ so that $\omega_1 - \omega_2 = 2\varepsilon$, we obtain from (3.1)

$$G(\omega + \varepsilon) - G(\omega - \varepsilon) = \int_{-\infty}^{\infty} e^{-j\omega t} \frac{e^{j\varepsilon t} - e^{-j\varepsilon t}}{jt} x(t)dt$$

$$G(\omega + \varepsilon) - G(\omega - \varepsilon) = \int_{-\infty}^{\infty} 2\frac{\sin(\varepsilon t)}{t} x(t) e^{-j\omega t} dt$$

This means that $G(\omega+\varepsilon) - G(\omega-\varepsilon)$ is the ordinary Fourier transform of the process $2x(t)\frac{\sin(\varepsilon t)}{t}$, which means:

$$\frac{\sin(\varepsilon t)}{\varepsilon t} x(t) = \frac{1}{2\pi} \int_{-\infty}^{\infty} e^{j\omega t} \frac{G(\omega+\varepsilon) - G(\omega-\varepsilon)}{2\varepsilon} d\omega \tag{3.3}$$

With $\varepsilon \to 0$, the left hand side tends to $x(t)$.

In order to give a system interpretation to $G(\omega)$, consider an ideal band-pass filter in Fig. 3.3:

$$H_{\omega_1\omega_2}(j\omega) = \begin{cases} 2\pi & \omega_2 < \omega < \omega_1 \\ 0 & elsewhere \end{cases}$$

Its impulse response is given as:

$$h_{\omega_1\omega_2}(t) = \frac{2\pi}{2\pi}\int_{\omega_2}^{\omega_1} e^{j\omega t} d\omega = \frac{e^{j\omega_1 t} - e^{j\omega_2 t}}{jt}$$

With $x(t)$ as input to this system, the output $y_{\omega_1\omega_2}(t)$ is given by convolution summation as:

$$y_{\omega_1\omega_2}(t) = \int_{-\infty}^{\infty} \frac{e^{j\omega_1(t-\tau)} - e^{j\omega_2(t-\tau)}}{j(t-\tau)} x(\tau) d\tau$$

At $t = 0$, the output will be

$$y_{\omega_1\omega_2}(0) = \int_{-\infty}^{\infty} \frac{e^{-j\omega_1\tau} - e^{-j\omega_2\tau}}{-j\tau} x(\tau) d\tau = G(\omega_1) - G(\omega_2)$$

In the same way if $\omega_1 > \omega_2 \geq \omega_3 > \omega_4 \geq \omega_5 > \omega_6$, then we can form systems as shown in Fig. 3.4. Clearly, these systems are disjoint. Therefore, with $x(t)$ as common input, the resulting outputs are orthogonal processes. Therefore,

$$E\left\{ y_{\omega_1\omega_2}(0) y^*_{\omega_3\omega_4}(0) \right\} = E\{[G(\omega_1) - G(\omega_2)]\,[G^*(\omega_3) - G^*(\omega_4)]\} = 0 \qquad (3.4a)$$

$$E\left\{ y_{\omega_3\omega_4}(0) y^*_{\omega_5\omega_6}(0) \right\} = E\{[G(\omega_3) - G(\omega_4)]\,[G^*(\omega_5) - G^*(\omega_6)]\} = 0 \qquad (3.4b)$$

It should, however be noted that $\omega_3 - \omega_4$ or $\omega_5 - \omega_6$ may or may not be equal to $\omega_1 - \omega_2$, that is, the systems do not necessarily have the same bandwidth. In other words, this leads to decomposing the signal into subbands. Returning to Fig. 3.4, if we make a bank of those bandpass filters with equal bandwidth of 2ε, then we have decomposition of the signal into uniform subbands as shown in Fig. 3.5. Likewise, we can have non-uniform subband

decomposition if we can vary the bandwidth of the filter in Fig. 3.3 for each system in Fig. 3.4, as shown in Fig. 3.6.

For discrete signal $x(n)$ and M discrete bandpass filters as in Fig. 3.4, then the output from bank of M bandpass filters, we have[27]:

$$y_k(n) = \sum_{m=-\infty}^{\infty} x(m)h(n-m)e^{2jk(n-m)\varepsilon} = c_k(n) \qquad k = 0, 1, \ldots, M-1$$

where ω_o is user-defined bandwidth of each bandpass filter. For ideal bandpass filters with user-defined bandwidth $2\varepsilon = \omega_o$, the above equation becomes:

$$y_k(n) = \sum_{m=-\infty}^{\infty} x(m)\frac{\sin[(n-m)\omega_o]}{(n-m)\pi}e^{jk(n-m)\omega_o} = c_k(n) \qquad (3.5a)$$

If we divide signal spectrum 2π by bandpass filter bandwidth ω_o then we have a bank of total L filters i.e., $L = \frac{2\pi}{\omega_o}$. The ability of the above equation to operate at different values (or scales) of L makes it efficient technique to decompose signal into various bands using filters of an ideal frequency response. In another way, we can say that we are decomposing the signals using discrete wavelet transform employing filters of an ideal frequency response. For $n = 0$, the above equation reduces to approximate Fourier expansion (AFE) of discrete signals[18].

$$c_k(0) = \sum_{m=-\infty}^{\infty} x(m)\frac{\sin\left(\frac{m\omega_o}{2}\right)}{m\pi}e^{-jkm\omega_o} = c_k \qquad (3.5b)$$

The equation (3.5a) means that we are decomposing the signal using AFE into M subbands. If $\omega_o = \frac{2\pi}{L}$ and L varies with the values to the logarithmic base of 2 with maximum value of M where M is a number of bandpass filters, then equation (3.5a) produces non-uniform subband decomposition of the signal as shown in Fig. 3.7. For $L = 2$, this is equal to subband

decomposition of the signal using filters of an ideal frequency response. Since this process generates two subbands, one with low frequency content and the other with high frequency content of the signal, the low frequency component can be further decomposed thus generating a dyadic tree decomposition. In other words, this is equivalent to applying successive subband decomposition on low-pass filtered signal at each decomposition level using approximate Fourier expansion (AFE). The signal can thus be represented by different resolutions at each level of the tree. The details of multiresolution signal decomposition can be found in reference [28]. The difference between multiresolution signal decomposition using wavelets or perfect reconstruction filters and signal decomposition using AFE is that latter reconstruct the original signal with an error depending on L. But the advantage of using AFE is that AFE can be implemented by an FFT algorithm.

After decomposing the signal, subbands can be represented by a transform to improve the representation efficiency. In particular, subbanding has proved to be useful when used in conjuction with several other techniques. For example, subbanding has been widely used with the discrete cosine transform (DCT) for image compression. The amount of improvement due to subbanding depends upon a number of factors such as energy distribution of the signal being considered, the choice of the frequency bands, the classes of signals in each band, etc. We will decompose 1-D signals and images in section 3.5.

3.4 Determination of Transformation Efficiency

In this section, we determine the efficiency of the trigonometric expansions by using first order Markov process. This model represents the gross behaviour of image sources moderately well, even though it fails if accurate modelling is required. Specifically, we will compute energy packing efficiency and the variance of the coefficients. In order to demonstrate the approach, we take first order Markov model as[29]:

$$\psi = \begin{bmatrix} 1 & \rho & \rho^2 & . & . & \rho^{N-1} \\ \rho & 1 & \rho & . & . & \rho^{N-2} \\ . & & & & & . \\ . & & & & & . \\ . & & & & & . \\ \rho^{N-1} & \rho^{N-2} & . & . & . & 1 \end{bmatrix}, \quad 0 < \rho < 1.$$

where ψ above provides a useful model for the data covariance matrix corresponding to the rows and columns of an image matrix and ρ is inter-element correlation coefficient. The covariance matrix in the transform domain is denoted by Ψ and is given by[30]:

$$\Psi = \Lambda \psi \Lambda^{*T} \tag{3.6}$$

where Λ is the 2-D matrix representation of a transform and Λ^* is its complex conjugate. Since AFE and ACE expansions have non-orthogonal basis functions and DFT and DCT are orthogonal transforms, we compare transform efficiency using equal number of transform coefficients i.e., $L = N$. The basis functions of AFE and ACE for N=8 and L=8 are computed from following equations (see equation (2.14) and (2.31)):

$$AFE: \quad c_{k,n} = \frac{\sin\left(\frac{n\pi}{L}\right)}{n\pi} e^{-j\frac{2\pi kn}{L}} \tag{3.7a}$$

$$ACE: \quad c_{k,n} = 2\frac{\sin\left(\frac{n\pi}{2L}\right)}{n\pi}\cos\left[\frac{\pi k(2n+1)}{2L}\right] \tag{3.7b}$$

$$DFT: \quad c_{k,n} = \frac{1}{\sqrt{(N)}}e^{-j\frac{2\pi kn}{N}} \tag{3.7c}$$

$$DCT: \quad c_{k,n} = C_o\sqrt{\frac{2}{N}}\cos\left[\frac{\pi k(2n+1)}{2N}\right] \quad where \quad C_o = \frac{1}{\sqrt{2}} \text{ if } k=0, \text{ and } 1 \text{ otherwise} \tag{3.7d}$$

The computed basis functions are shown in Table 1. We determine the transform efficiency of AFE, ACE, DFT and DCT by examining the diagonal elements of their respective transform domain covariance equation (19) (for $\rho = 0.91$, N=16 and L=16), where Λ represents respective transformation matrix. The relative amount of energy in the first M of the total N diagonal components is given as[29]:

$$\eta_{transform} = \frac{\sum_{j,k=1}^{M} Y_{j,k}}{\sum_{j,k=1}^{N} X_{j,k}}, \quad j = k \tag{3.8}$$

where $\sum X_{j,k}$ is total sum of data covariance entries and $\sum Y_{j,k}$ is total sum of transform covariances. We calculated the energy packing efficiency of DCT, DFT, ACE and AFE by looking at diagonal elements of their transform covariance matrices when $j = k$ and M varies from 1 to N and results are shown in Fig. 3.8. The best performance is given by ACE followed closely by DCT and AFE. The larger values of η, even for relatively small values of M, are characteristics of all transforms and are the result of high inter-element correlation within the data. Good energy packing efficiency also demands that the magnitudes of the variances fall off rapidly with increasing coefficient order. In order to compare transform coefficient variances of DCT, DFT and approximate trigonometric expansions, we again analyzed the

diagonal elements of their respective transform domain covariance matrices. The diagonal elements of each transform domain covariance matrix are shown in Fig. 3.9 which shows that the performance of ACE is the best followed by DCT and AFE. Owing to the symmetry inherent within the basis matrix, the AFE and DFT have pairs of coefficients of equal variance, and this accounts for the step-like trend of their curves. In order to demonstrate decorrelation efficiency of trigonometric expansions, we use the same first order Markov model by calculating the decrease in inter-element correlation in transform domain covariance matrix compared with that in data domain equivalent. The decorrelation efficiency is then given as[29]:

$$\eta_{decorrelation} = 1 - \frac{\sum_{j,k=1}^{N} Y_{j,k}}{\sum_{j,k=1}^{N} X_{j,k}}, \quad j \neq k \tag{3.9}$$

where $\sum X_{j,k}$ and $\sum Y_{j,k}$ are defined as above. We computed the decorrelation efficiency of approximate trigonometric expansions, discrete cosine and Fourier transforms for various values of N and ρ and the results are shown in Table 2. It is clear from the Table 2 that approximate trigonometric expansions provide better inter-element decorrelation than discrete cosine and Fourier transforms.

Multispectral imagery has been used in geological applications to study the composition and dynamics of earth surfaces in cartography, mineral exploration, analysis of land utilization, weather and climate analysis, as well as agriculture and forestry applications. In most systems the image acquired by the senser is transmitted to a processing center on earth. Significant research has taken place in techniques for compression of such images, as well as processing to recognize patterns of interest. In addition to using correlation between the

different pixels of the image in one spectral band, techniques have also been invented to utilize the cross correlation between the images in different spectral bands. Single band image compression relies mainly upon the spatial correlation of the image pixels to accompolish this task. Multiple, correlated spectral bands provide a third dimension in which redundancy can be exploited. This band to band redundancy permits one to apply various redundancy removing techniques. Examples of techniques applied to multispectral imagery include three-dimensional prediction technique[1], spectral prediction followed by spatial decorrelation step like block discrete cosine transform (DCT) technique[2], and spectral decorrelation transform techniques[3]. A comparative performance evaluation of various multispectral compression techniques is given in [37]. In general, transform based techniques outperform the classical predictive methods. A robust implementable compression algorithm for multispectral imagery with a selectable quality level is reported in [38]. This techniques employs one-dimensional Karhunen-Loeve transform (KLT) followed by two-dimensional block discrete cosine transform (DCT). The multispectral image set is spectrally decorrelated via the KLT to produce the eigen images. The resulting decorrelated images are then compressed using the JPEG algorithm. Since the KLT is data dependent therefore this algorithm is computationally intensive. In addition it adds an overhead information (like covariance matrix and eigen values) to the compressed imagery which needs to be transmitted to the decoder for correct reconstruction. A practical transform for the purpose of signal compression should have a strong decorrelating effect, should preferably consist of signal-independent basis functions, and should have a fast implementation. In order to demonstrate the spectral decorrelation across bands, we apply an approximate cosine expansion to a multispectral image set. In this experiment, ten spectrally correlated images,

each of size 256x256 with 8 bits per pixel, were used. Figure 3.10 shows two sample images used in this experiment. From a set of ten spectrally correlated images, each vector from spectrally correlated components from identical locations in each band is formed and an approximate cosine expansion (ACE) applied on it. The resulting output vectors are placed adjacent to one another, in the same order as the input vectors, to form the stack of the spectrally decorrelated image planes. Figure 3.11 shows first four spectrally decorrelated image planes associated with ten-band test image set. From Figure 3.11, the compaction of data as a result of approximate cosine expansion is clearly evident as first two image planes contain significant amount of energy or information content. The remaining decorrelated image planes contain very little information and thus require substantially fewer bits to be coded. It should, however, be noted that relatively higher values of N would produce better results because relatively higher values of N yield better decorrelation between output vector elements as shown in Table 3.2. In order to measure the spectral decorrelation, the correlation coefficient is computed across each pair of spectrally decorrelated image planes. The correlation coefficient is a useful and convenient method to measure the inherent spectral correlation[33]. The correlation coefficient matrix is defined as the normalized covariance matrix i.e., the coefficient for each pair of bands is equal to their covariance value divided by the square root of the product of their individual variances. The computed correlation coefficient across each pair of spectrally decorrelated bands is shown in Table 3.3*a*. For comparison purposes, DCT was also applied on multispectral image set and correlation coefficient computed across each pair of spectrally decorrelated bands. The result is shown in Table 3.3*b*. It is clear from Table 3.3*a* that the approximate cosine expansion (ACE) provides relatively better spectral decorrelation efficiency than discrete cosine transform

(DCT).

In most practical situations, some amount of signal degradation can be tolerated. This poses a question, which is, what is the minimum bit rate required to encode a source while keeping the degradation below a certain level. The performance criterion for a coding scheme can also be measured by the minimum information rate R that can be achieved while still maintaining a fixed distortion D within the framework of the basis-restricted structure. Considering Gaussian sources along with the mean-square criterion, the rate-distortion performance criterion is given as[31]:

$$R(D) = \frac{1}{2M} \sum_{j=1}^{M} \max\left\{0, \ln\left(\frac{\sigma_j}{\theta}\right)\right\} \tag{3.10a}$$

$$D = \frac{1}{M} \sum_{j=1}^{M} \min(\theta, \sigma_j) \tag{3.10b}$$

where θ is distortion variable and the σ_j are the main diagonal terms of the transform domain covariance matrix Ψ in equation (3.6). We implemented equation (3.10*a*) and (3.10*b*) for AFE, DFT and DCT using equation (3.6) for M=16 and $\rho = 0.9$, and the results are shown in Fig. 3.12, from which it is clear that the performance of ACE is the best followed by DCT and AFE.

3.5 Simulations

In this section, we present experimental results. In section 3.2, we briefly discussed multiresolution signal decomposition using wavelets. Specifically, we described Mallat's discrete wavelet transform algorithm known as fast wavelet transform. Furthermore, we explored the capability of the approximate Fourier expansion as a signal decomposition tool. In this section, we apply an approximate Fourier expansion (AFE) on 1-D signals and images in a manner similar to fast wavelet transform. As an example of 1-D signal, we used a segment with the length of 256 samples, of a speech signal and applied equation (3.5), on it, similar to non-uniform subband decomposition as shown in Fig. 3.7. In similar fashion, we applied equation (3.5) on "Lena" and "Shipyard" images. The approach, applied on each image and the segment of a speech signal, is as follows:

Step 1: Equation (3.5) with L=2 is applied on an image in horizontal direction. This produces two output images. Since L=2, hence filtered output images have bandwidth of $\omega_o = \frac{2\pi}{L} = \pi$ in horizontal direction.

Step 2: Since one signal has maximum frequency of π, and another is confined between π and 2π, therefore both signals can be decimated by L=2.

Step 3: The steps 1 and 2 are repeated on both images in vertical direction. This process generates total four images.

Step 4: The steps 1,2 and 3 can be applied repeatedly on lowpass filtered images as desired.

Step 5: Depending on the signal characteristics of the image at any level of decomposition, individual filtered subimages can be transform-coded using the approximate cosine

expansion (ACE) with L equal to the size of the subimage.

Step 6: For reconstruction, each lower level can be reconstructed from its immediate higher level by the process inverse to steps 1,2,3,4 and 5.

The results are shown in Fig. 3.13 through Fig. 3.16 for four levels of decomposition, and the corresponding reconstructed signals. Fig. 3.13 shows original, decomposed, and reconstructed signal of the segment of a speech signal under test. Fig. 3.13*a* shows a segment (N=256) of original speech signal where as Fig. 3.13*b*, Fig. 3.13*c*, Fig. 3.13*d*, Fig. 3.13*e*, Fig. 3.13*f*, and Fig. 3.13*g* show decomposed signals corresponding to four levels of decomposition, and Fig. 3.13*h* shows reconstructed signal using the inverse process in a similar way as shown in Fig. 3.2. In the same way, the results for "Lena" image and "Shipyard" image are shown in Fig. 3.15 and Fig. 3.16 respectively.

From above simulations, it can be observed that each decomposition of the signal generates a high-band signal, which, in most of the cases of signal coding applications, can be coarsely quantized. In section 3.4, we showed that for first order Markov processes and spectral decorrelation across bands in a multispectral imagery, the decorrelation efficiency and transform efficiency of the approximate cosine expansion (ACE) is better than the discrete cosine transform. This implies that, in a low bit rate application, decomposed signals can be represented by the approximate cosine expansion (ACE) for the purpose of coding. We will apply an approximate cosine expansion (ACE) to the decomposed signals in the next chapter.

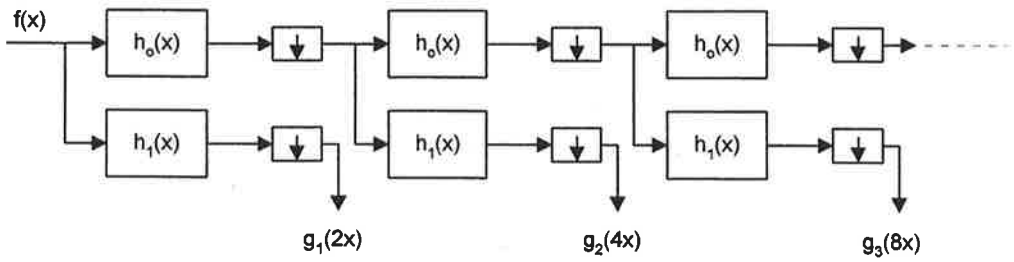

Fig. 3.1. Forward fast wavelet transform algorithm

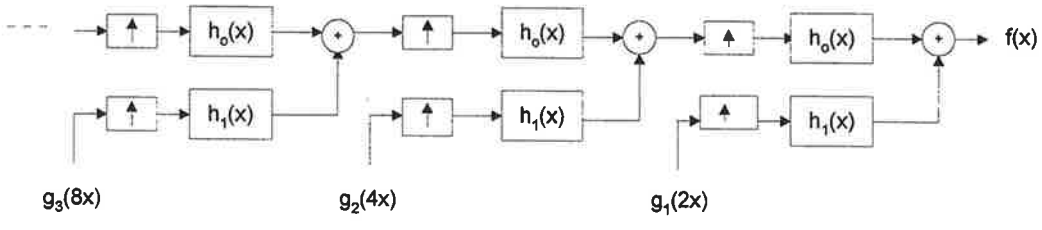

Fig. 3.2. Inverse fast wavelet transform algorithm

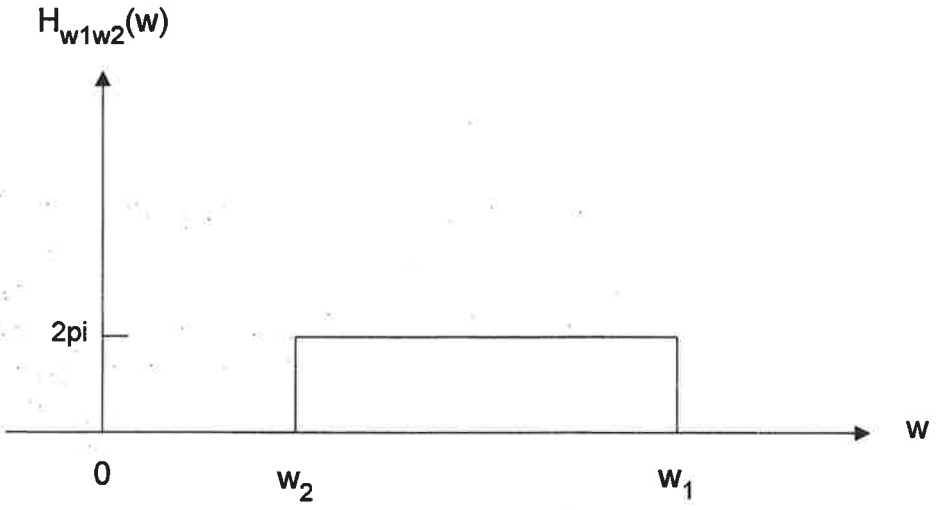

Fig. 3.3. Ideal bandpass filter

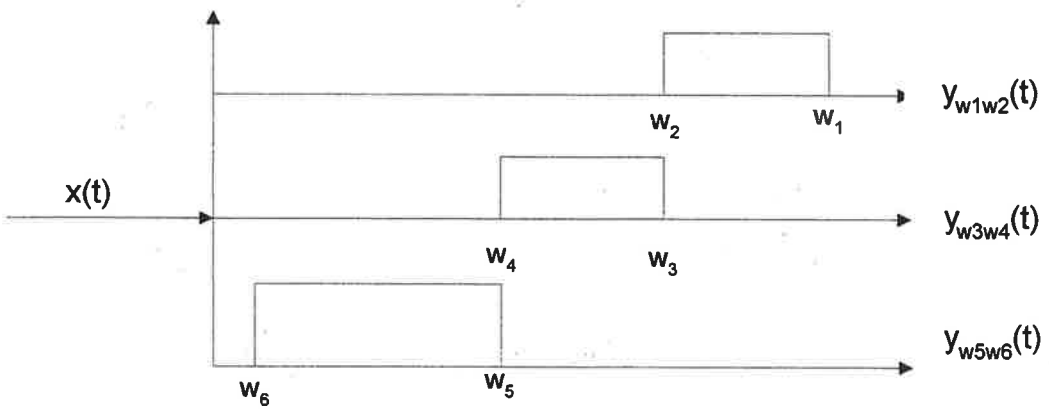

Fig. 3.4. A bank of bandpass filters

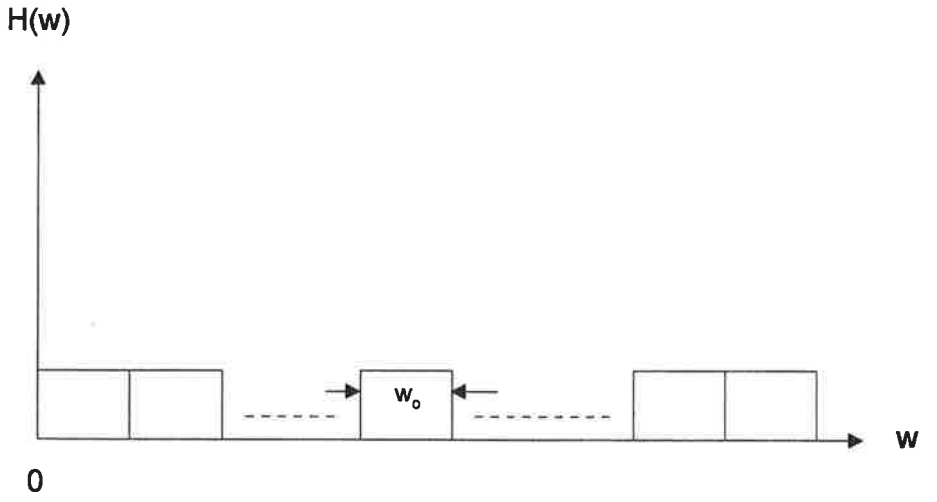

Fig. 3.5. Uniform subband decomposition

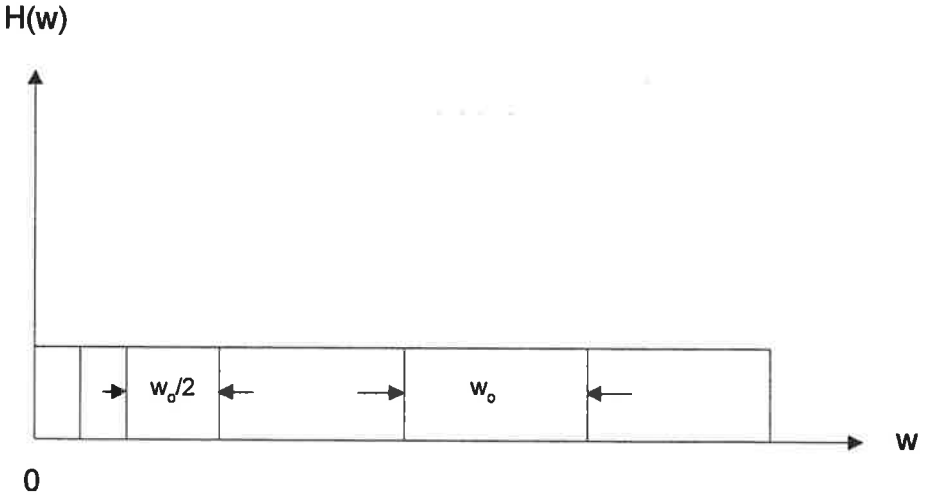

Fig. 3.6. Non-uniform subband decomposition

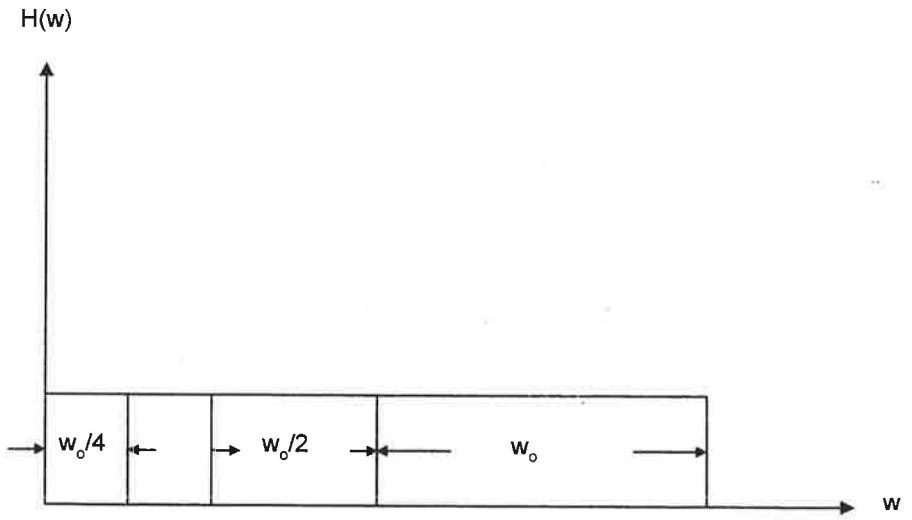

Fig. 3.7. Dyadic tree decomposition

0.0892	0.1059	0.1179	0.1242	0.1242	0.1179	0.1059	0.0892
0.0892	0.0749	0	−0.0878	−0.1242	−0.0834	0	0.0631
0.0892	0	−0.1179	0	0.1242	0	−0.0159	0
0.0892	−0.0749	0	0.0878	−0.1242	0.0834	0	−0.0631
0.0892	−0.1059	0.1179	−0.1242	0.1242	−0.1179	0.1059	−0.0892
0.0892	−0.0749	0	0.0878	−0.1242	0.0834	0	−0.0631
0.0892	0	−0.1179	0	0.1242	0	−0.1059	0
0.0892	0.0749	0	−0.0878	−0.1242	−0.0834	0	0.0631

Table 3.1a. Real part of AFE basis functions, N=8, L=8

0	0	0	0	0	0	0	0
0	−0.0749	−0.1179	−0.0878	0	0.0834	0.1059	0.0631
0	−0.1059	0	0.1242	0	−0.1179	0	0.0892
0	−0.0749	0.1179	−0.0878	0	0.0834	−0.1059	0.0631
0	0	0	0	0	0	0	0
0	0.0749	−0.1179	0.0878	0	−0.0834	0.1059	−0.0631
0	0.1059	0	−0.1242	0	0.1179	0	−0.0892
0	0.0749	0.1179	0.0878	0	−0.0834	−0.1059	−0.0631

Table 3.1b. Imaginary part of AFE basis functions, N=8, L=8

0.1154	0.12	0.1232	0.1248	0.1248	0.1232	0.12	0.1154
0.1132	0.0998	0.0684	0.0243	−0.0243	−0.0684	−0.0998	−0.1132
0.1066	0.0459	−0.0471	−0.1153	−0.1153	−0.0471	0.0459	0.1066
0.0959	−0.0234	−0.1208	−0.0693	0.0693	0.1208	0.0234	−0.0959
0.0816	−0.0849	−0.0871	0.0822	0.0882	−0.0871	−0.0849	0.0816
0.0641	−0.1177	0.024	0.1038	−0.1083	−0.024	0.1177	−0.0641
0.0442	−0.1109	0.1138	−0.0478	−0.0478	0.1138	−0.1109	0.0442
0.0225	−0.0667	0.1024	−0.1224	0.1224	−0.1024	0.0667	−0.0225

Table 3.1c. ACE basis functions, N=8, L=8

0.3536	0.3536	0.3536	0.3536	0.3536	0.3536	0.3536	0.35536
0.3536	0.25	0	−0.25	−0.3536	−0.25	0	0.25
0.3536	0	−0.3536	0	0.3536	0	−0.3536	0
0.3536	−0.25	0	0.25	−0.3536	0.25	0	−0.25
0.3536	−0.3536	0.3536	−0.3536	0.3536	−0.3536	0.3536	−0.3536
0.3536	−0.25	0	0.25	−0.3536	0.25	0	−0.25
0.3536	0	−0.3536	0	0.3536	0	−0.3536	0
0.3536	0.25	0	−0.25	−0.3536	−0.25	0	0.25

Table 3.1d. Real part of DFT basis functions, N=8

0	0	0	0	0	0	0	0
0	0.25	0.3536	0.25	0	−0.25	−0.3536	−0.25
0	0.3536	0	−0.3536	0	0.3536	0	−0.3536
0	0.25	−0.3536	0.25	0	−0.25	0.3536	−0.25
0	0	0	0	0	0	0	0
0	−0.25	0.3536	−0.25	0	0.25	−0.3536	0.25
0	−0.3536	0	0.3536	0	−0.3536	0	0.3536
0	−0.25	−0.3536	−0.25	0	0.25	0.3536	0.25

Table 3.1e. Imaginary part of DFT basis functions, N=8

0.3536	0.3536	0.3536	0.3536	0.3536	0.3536	0.3536	0.3536
0.4904	0.4157	0.2778	0.0975	−0.0975	−0.2778	−0.4157	−0.4904
0.4619	0.1913	−0.1913	−0.4619	−0.4619	−0.1913	0.1913	0.4619
0.4175	−0.0975	−0.4904	−0.2778	0.2778	0.4904	0.0975	−0.4157
0.3536	−0.3536	−0.3536	0.3536	0.3536	−0.3536	−0.3536	0.3536
0.2778	−0.4904	0.0975	0.4157	−0.4157	−0.0975	0.4904	−0.2778
0.1913	−0.4619	0.4619	−0.1913	−0.1913	0.4619	−0.4619	0.1913
0.0975	−0.2778	0.4157	−0.4904	0.4904	−0.4157	0.2778	−0.0975

Table 3.1f. DCT basis functions, N=8

	N=8				N=16				N=32			
ρ	0.85	0.9	0.95	0.98	0.85	0.9	0.95	0.98	0.8	0.9	0.95	0.98
DFT	0.831	0.883	0.94	0.975	0.782	0.839	0.911	0.962	0.772	0.816	0.886	0.948
DCT	0.966	0.978	0.989	0.995	0.963	0.976	0.988	0.995	0.962	0.975	0.988	0.995
AFE	0.982	0.986	0.99	0.992	0.991	0.993	0.995	0.997	0.996	0.996	0.997	0.998
ACE	0.996	0.997	0.998	0.998	0.998	0.998	0.999	0.999	0.999	0.999	0.999	0.999

Table 3.2. Decorrelation efficiency of ACE/DCT/AFE/DFT for various values of inter-element correlation

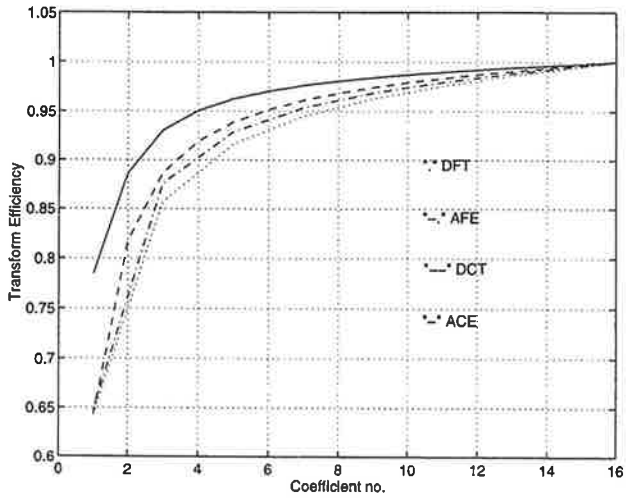

Fig. 3.8 Energy packing efficiency of ACE/DCT/AFE/DFT

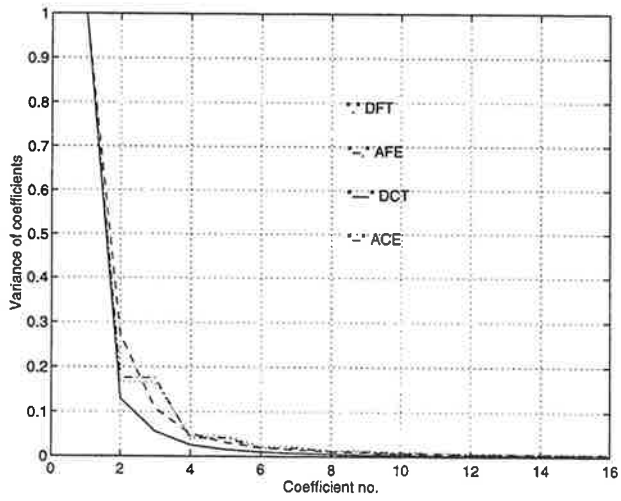

Fig. 3.9 Variance of ACE/DCT/AFE/DFT

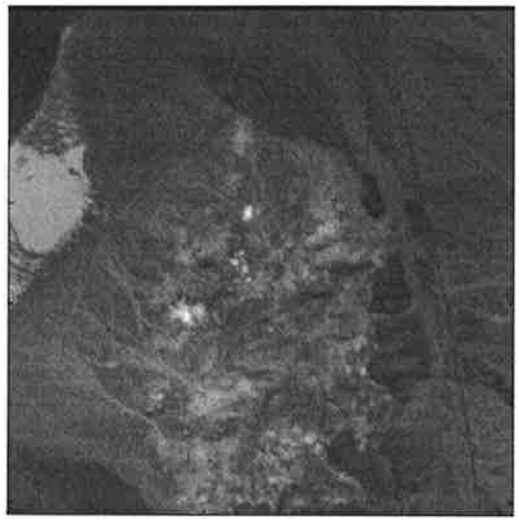

Fig. 3.10*a* Sample multispectral image (Band 1)

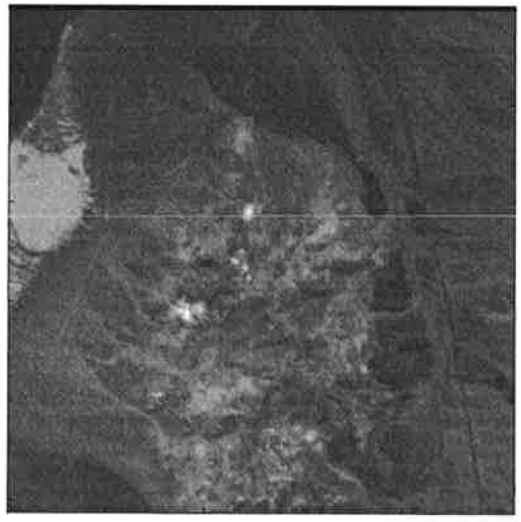

Fig. 3.10*b* Sample multispectral image (Band 2)

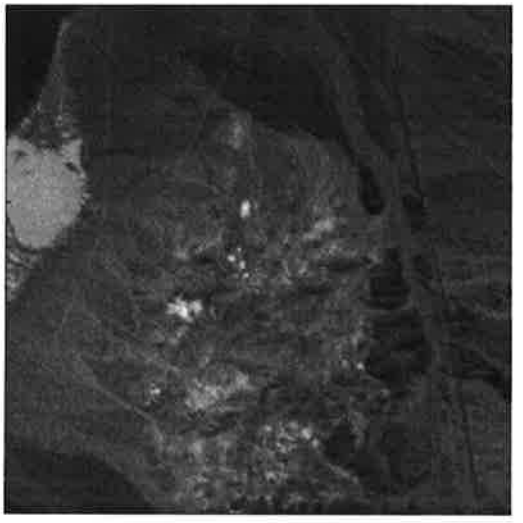

Fig. 3.10*c* Sample multispectral image (Band 3)

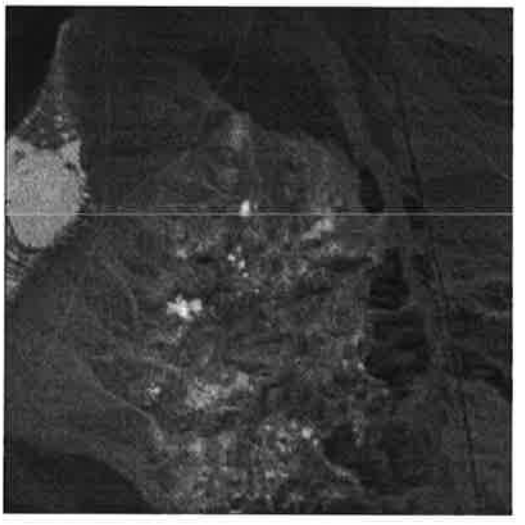

Fig. 3.10*d* Sample multispectral image (Band 4)

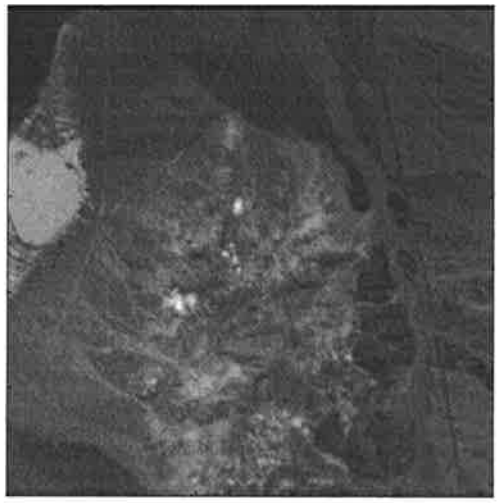

Fig. 3.11*a* First spectrally decorrelated image

Fig. 3.11*b* Second spectrally decorrelated image

Fig. 3.11*c* Third spectrally decorrelated image

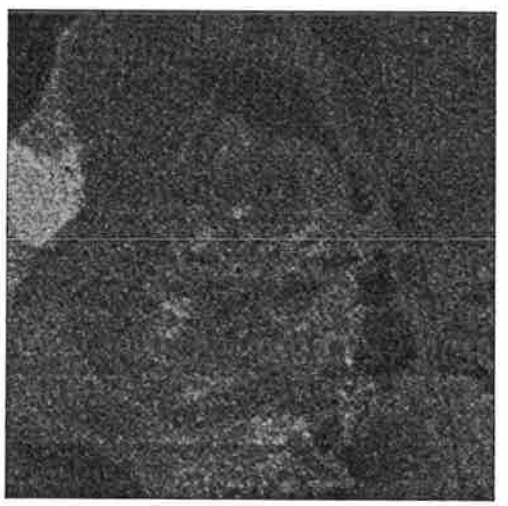

Fig. 3.11*d* Fourth spectrally decorrelated image

	1	2	3	4	5	6	7	8	9	10
1	1									
2	0.888	1								
3	0.912	0.927	1							
4	0.829	0.925	0.853	1						
5	0.881	0.918	0.915	0.882	1					
6	0.710	0.831	0.709	0.857	0.782	1				
7	0.838	0.885	0.884	0.780	0.819	0.679	1			
8	0.175	0.354	0.127	0.507	0.247	0.594	0.156	1		
9	0.720	0.743	0.761	0.693	0.721	0.571	0.627	0.129	1	
10	0.321	0.146	0.397	0.043	0.244	0.232	0.350	0.204	0.297	1

	1	2	3	4	5	6	7	8	9	10
1	1									
2	0.918	1								
3	0.914	0.961	1							
4	0.905	0.950	0.943	1						
5	0.895	0.932	0.927	0.933	1					
6	0.873	0.912	0.904	0.893	0.907	1				
7	0.855	0.893	0.896	0.867	0.841	0.857	1			
8	0.801	0.828	0.838	0.816	0.799	0.747	0.815	1		
9	0.739	0.778	0.775	0.768	0.740	0.727	0.663	0.692	1	
10	0.326	0.328	0.394	0.218	0.252	0.234	0.352	0.267	0.302	1

Table 3.3 Correlation coefficient across bands (Top table: ACE, Bottom table: DCT)

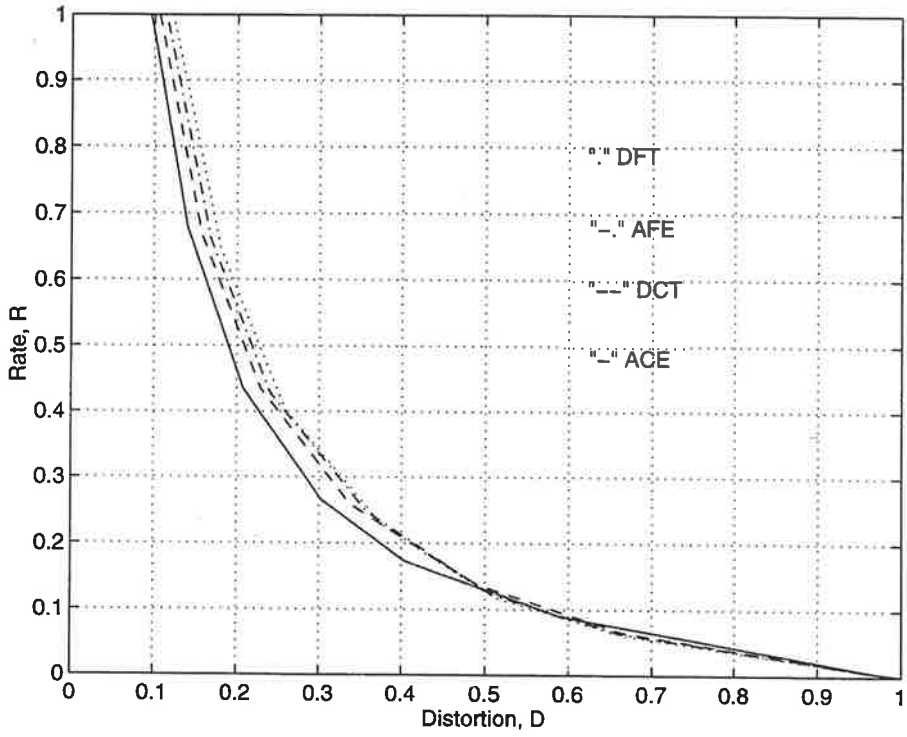

Fig. 3.12 Rate vs. Distortion relation of ACE/DCT/AFE/DFT

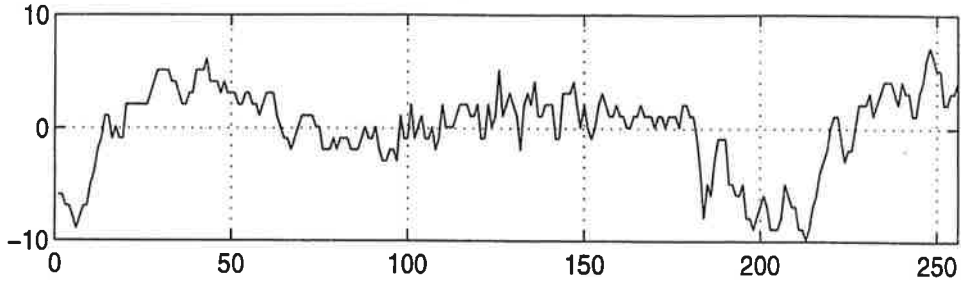

Fig. 3.13*a* Original segment of speech signal

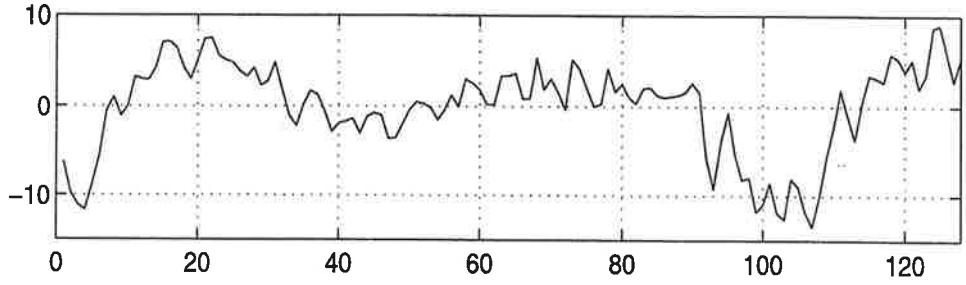

Fig. 3.13*b* Low band signal after first decomposition

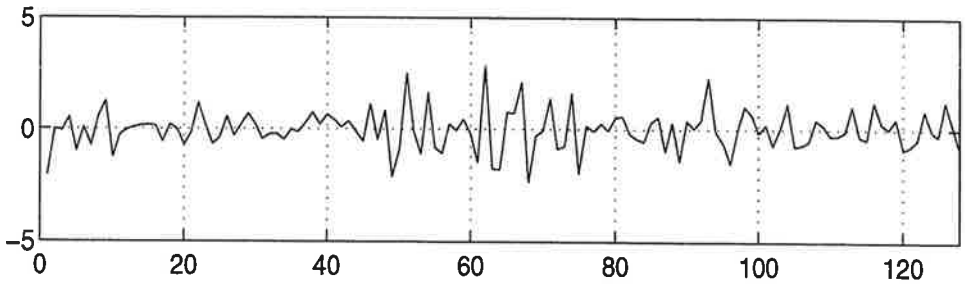

Fig. 3.13*c* High band signal after first decomposition

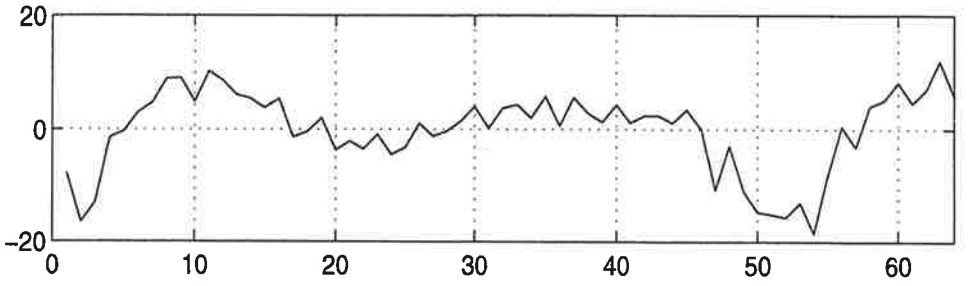

Fig. 3.13*d* Low band signal after second decomposition

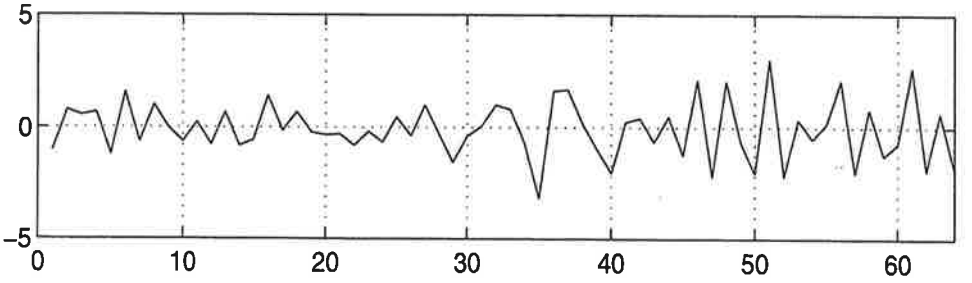

Fig. 3.13*e* High band signal after second decomposition

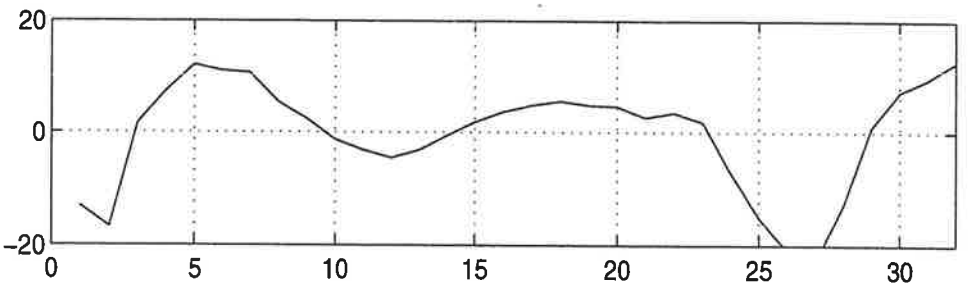

Fig. 3.13*f* Low band signal after third decomposition

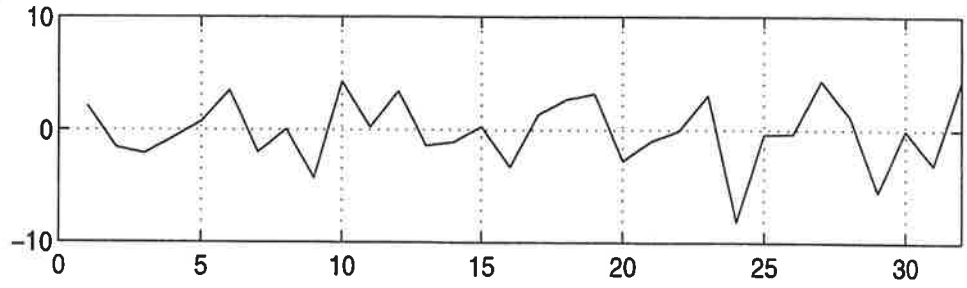

Fig. 3.13*g* High band signal after third decomposition

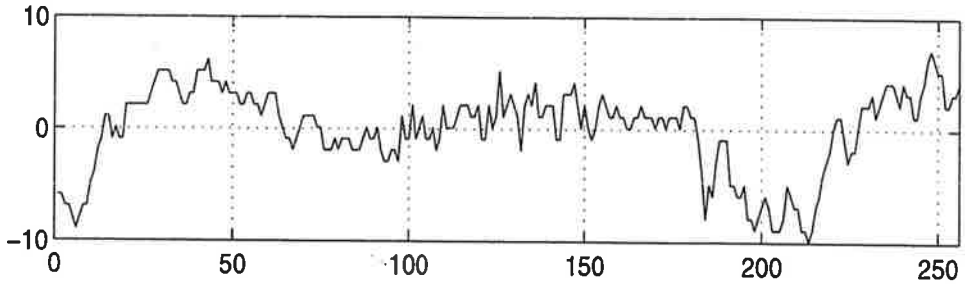

Fig. 3.13*h* Signal after reconstruction

Fig. 3.14 Original "Lena" image

Fig. 3.15*a* Decomposed "Lena" image with four levels

Fig. 3.15*b* Reconstructed "Lena" image

Fig. 3.16*a* Original "Shipyard" image

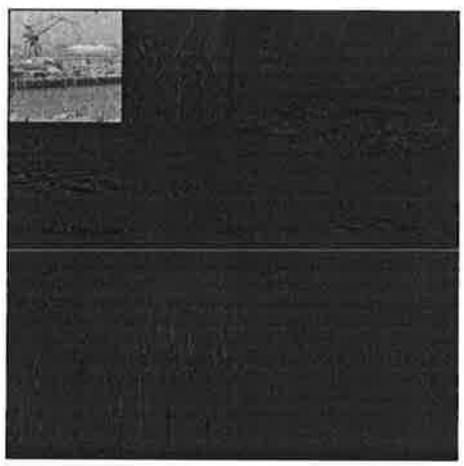

Fig. 3.16*b* Decomposed "Shipyard" image with four levels

Fig. 3.16*c* Reconstructed "Shipyard" image

4. COMPRESSION OF SIGNALS USING THE APPROXIMATE TRIGONOMETRIC EXPANSIONS

4.1 Background

Signal compression is achieved in two stages. The first is the basic representation level, where the energy is compacted in the fewest number of coefficients, and the second is the coding of these coefficients. The first three chapters of this research dealt with the first stage of signal compression i.e., discussion and analysis of the existing signal representation techniques as well as proposed method using the approximate trigonometric expansions. The second stage involves the coding of the resulting coefficients using an appropriate coding scheme. The main goal in this part of the research is explore the capability of the trigonometric expansions for coding of multidimensional signals.

With a good coding scheme degradations are subtle, and their perception and impact changes from observer to observer, being dependent upon a host of individual and environmental parameters probably impossible to characterize consistently. The old arguments about the drawbacks of a mean square error (m.s.e) measure and its vague relationship with perceived picture quality are still valid, of course, and their are enough reports in the literature to correlate these two quantities in a positive direction to confirm this. The other measure used is signal-to-noise-ratio (SNR). A decade ago there was no consistency in the literature regarding an appropriate form of SNR to use for this purpose[29]: the following three are possibilities[32]:

$$10\log_{10}\frac{\sigma_x^2}{\frac{1}{N^2}\sum_{image}(x-\hat{x})^2} \quad \text{dB} \tag{4.1}$$

$$10\log_{10}\frac{\sum_{image} x^2}{\sum_{image}(x-\hat{x})^2} \quad \text{dB} \tag{4.2}$$

$$10\log_{10}\frac{x_{max}^2}{\frac{1}{N^2}\sum_{image}(x-\hat{x})^2} \quad \text{dB} \tag{4.3}$$

where there are N^2 elements in the image, x and $\hat{x}$ are arbitrary original and reconstructed signal elements, respectively, and σ^2 is the variance of the input image. The equation (4.1) relates the m.s.e to the image variance, the equation (4.2) relates it to image mean square energy, and equation (4.3) also called Peak SNR or PSNR relates it to maximum image energy (x=255 for an 8 bit image). With the move to an increased degree of interest in video coding, the equation (4.3) has become more common although the other two are occasionally used. In this research we will compare reconstructed signals and images using equations (4.2) and (4.3).

Historically, there have been two ways in which selection of coefficients for further processing can be carried out. The first, zonal coding, involves the setting up of a number of zones of predetermined bit allocation, according to some coefficient energy versus error relation. The results obtained are, however, variable. But the drawback of this technique is that it takes no account of local variability of coefficient magnitudes because some of the coefficient blocks may correspond to signal blocks containing very active spatial activity. The alternative technique, threshold coding, establishes set of thresholds and coefficients larger than a predetermined level(s) are saved and processed further, those smaller being

deleted. Since larger coefficients are expected to contribute proportionally more to signal activity, this technique seems to be logical. But it has its disadvantage i.e., the decoder needs the addresses of the coefficients retained before their transmission or storage. However, this is the method which has been chosen for the still picture coding standard. In this research, we will also employ threshold coding to transformed signals and images.

4.2 Simulation-I

In chapter 3, we explored the capability of the approximate Fourier expansion (AFE) for signal decomposition of the signals. In this section, we will apply an approximate cosine expansion (ACE) to decomposed speech signals for the purpose of compression. For the purpose of comparison, the discrete cosine transform (DCT) will also be applied to decomposed signals.

We used three speech signals each sampled at 22kHz, with 8 bits per sample and PCM (pulse code modulation) format. The speech signals are:

1. "Original".
2. "This is the end of the demonstration".
3. "In the five demonstrations that follow, the original signals where first processed with the window size of 11, then reprocessed with the window size of 25 and finally processed again with the window size of 37".

In the simulation, (N=256) samples were considered for block processsing. Each of these blocks of speech signals is decomposed into 3 decomposition levels using an

approximate Fourier expansion (AFE) with L=2. The number of decomposition levels chosen was arbitrary. The method applied for decomposition is similar as described in section 3.5. In this method, the low frequencies have a smaller frequency band as compared to the higher frequencies. This is specially useful for certain classes of signals e.g., voiced speech signals where the energy is concentrated at lower frequencies. It may be noted that band ranges for optimal compression are bound to vary according to signal statistics. Furthermore, the decomposed signals were subjected to following actions:

1. Band 3 (128 samples) contains very little energy, and therefore was set to zero.
2. Band 2 (64 samples) was represented by an ACE as well as DCT.
3. Band 1 (64 samples) was also represented by ACE as well as by DCT.

Before reconstructing the original block of the signal, the bands 1 and 2 were subjected to threshold coding depending upon the subjective and objective quality of the reconstructed signal. The different thresholds, each for DCT and ACE coefficients, were used to retain equal number of coefficients for comparison purposes. The following actions were taken on coefficients of all of the blocks of three speech signals:

1. Band 2: 96% coefficients were set to zero.
2. Band 1: 4% coefficients.

This way, we achieve a coefficient reduction ratio (CRR) of 4 to 1. The rest of the coefficients were inverse transformed to yield back both subbands which were then combined using

synthesis operation as described in section 3.5. In order to test the reconstructed signals using objective fidelity criterion, mean signal-to-noise-ratio (SNR_{ms}) and peak signal-to-noise-ratio (PSNR) were computed of each block and averaged across all of the signal blocks in each speech signal. The results are as follows:

	PSNR	SNR_{ms}
1. Signal-1:		
ACE:	27.2 *dB*	25.9 *dB*
DCT:	25.9 *dB*	24.5 *dB*
2. Signal-2:		
ACE:	34.3 *dB*	33.4 *dB*
DCT:	33.1 *dB*	32.3 *dB*
3. Signal-3:		
ACE:	30.9 *dB*	29.8 *dB*
DCT:	29.7 *dB*	28.5 *dB*

It is obvious that subband signals represented using an approximate cosine expansion (ACE) has higher SNR as compared to subbands represented by DCT in a constrained environment. Although, subband method employed uses filters of an ideal response i.e., they do not die out quickly from their central location, filters or wavelets of shorter length can be used for decomposing the signal into its subbands. The purpose here was to test that in a constrained environment, the ACE together with AFE can be used for representation of 1-D signals.

Subband representation using ACE can be compared also with DCT representation

when signals are decomposed using filters of shorter length like Daubechies 4 (db4). The filter coefficients for "db4" are plotted in Fig. 4.1. In order to demonstrate the approach, we use the same procedure as followed for signal decomposition using an approximate Fourier expansion with L=2, and the results based on objective fidelity criterion (like PSNR and SNR*ms*) of reconstructed signals are as follows:

	PSNR	SNR_{ms}
1. Signal-1:		
ACE:	30.5 *dB*	30 *dB*
DCT:	29 *dB*	28.6 *dB*
2. Signal-2:		
ACE:	30.9 *dB*	30.5 *dB*
DCT:	29.6 *dB*	28.4 *dB*
3. Signal-3:		
ACE:	30.4 *dB*	30.1 *dB*
DCT:	29 *dB*	28.8 *dB*

The improvement in signal-to-noise-ratio, in this case, can be attributed due to the fact that Daubechies wavelets use filters which die out quickly from their central location where as the approximate Fourier expansion (AFE) with L=2 uses filters which are (theoretically) of infinite length. The details of Daubechies wavelets of order N can be found in references [33]-[35].

4.3 Simulations-II

In previous section, we applied the approximate trigonometric expansions to speech signals for the purpose of compression. In this section, we explore the compression of images using the approximate trigonometric expansion. Based on local signal statistics, the user-defined parameter L can be varied for the purpose of decomposition of the image in question. The decomposed sub-images can further be represented by the approximate trigonometric expansions for the purpose of coding. For comparison purposes, the block discrete cosine transform will also be applied to images. Performance of the reconstructed images will be evaluated by signal-to-noise-ratio.

We used two images "Lena" and 'Shipyard" each of size 256x256 with 8 bits of resolution. Before decomposition of the test-images using ideal bandpass filters, we tested the approximate trigonometric expansions on the test-images and compared it with the discrete cosine transform. Three different thresholds, each for DCT, AFE and ACE coefficients, were used to retain equal number of coefficients. The number of coefficients retained was 10% of the total NxN coefficients for all of the three cases. Results are shown in Fig. 4.2 through 4.4. Poor SNR*ms* in Fig. 4.2*a* and Fig. 4.2*b* accounts mainly for windowing effect present in the reconstructed images. Furthermore, AFE has one more disadvantage: its coefficients are complex, which requires processing of real as well as imaginary coefficients. It is clear from Fig. 4.2, Fig. 4.3 and Fig. 4.4 that ACE has better performance than DCT and AFE. This verifies our results in sections 2.5,2.6 and 3.4. It should, however, be noted that further compression can be achieved by proper coding of the quantized coefficients such as Huffman and Runlength coding.

Previous transformation did not involve block processing of the test-images, and

therefore did not take the local signal characteristics into account. The second disadvantage is that the possible range of coefficient magnitude increases with transform order[29], and so, for a 256x256 transform, it is very large. The alternative approach, and more usual as suggessted in JPEG standard, is to use block transform. First the images are divided into subimages of typical size 16x16. These subimages are subjected to the approximate cosine expansion (ACE). For comparison, the discrete cosine transform (DCT) is also applied to these subimages. Depending upon the coefficient reduction ratio (CRR), the retained coefficients were multiplied with quantization matrix and then rounded. The number of coefficients retained was 10% of the total coefficients. For reconstruction, the rounded coefficients in each block were inverse transformed using inverse discrete cosine transform (IDCT) and synthesis equation as given in equation (2.32) to yield back the approximated original images. The signal-to-noise-ratio of reconstructed images was computed and the results are shown in Fig. 4.5 and Fig. 4.6. It is obvious from these Figures that the signal-to-noise-ratio of images coded using approximate cosine expansion (ACE) is higher than the images coded using the discrete cosine transform (DCT).

The block processing and coding of images, implemented as above, can further be improvised in two ways. First the test-images can be decomposed based on signal statistics, using ideal bandpass filters as discussed in chapter 3. Second the decomposed images can be represented by the approximate cosine expansion (ACE), and then a set of the coefficients can be retained and quantized in each transformed block according to signal statistics. We applied the procedure similar to as described in section 3.5. We decomposed each test-image into three levels. Each decomposition creates four subimages namely $a00$, $a01$, $a02$, $a03$. The decomposed images were subjected to following actions:

1. The subimages $a01$, $a02$, $a03$ of the first decomposition level were set to zero.
2. The subimages $a03$ of the second decomposition level was set to zero.
3. The subimages $a02$, $a01$ of the second decomposition level were transformed using the approximate cosine expansion with L equal to the size of the subimages. The number of coefficients retained was 30% of total 64x64 coefficients in each subimages.
4. The subimages $a01$, $a02$ and $a03$ of third decomposition were transformed using the approximate cosine expansion with L equal to the size of the subimages. The number of retained coefficients was 97% of the total 32x32 coefficients in each subimage.

The total number of coefficients/samples retained came out to be 10% of the total 256x256 samples in the image. For reconstruction, the process applied is inverse to that applied during decomposition and transformation of the subimages. The signal-to-noise-ratio of the reconstructed image was computed and the result is shown in Fig. 4.6. It is clear from Fig. 4.2 through Fig. 4.6 that the performance of ACE is better than DCT for the purpose of coding. Furthermore, the compression achieved due to ACE will be higher than due to DCT because the energy compaction of ACE is better than DCT as verified in section 3.4.

4.4 Simulations-III

In section 3.4, we discussed the removal of inherent spectral correlation in multispectral imagery using the spectral decorrelation transform techniques. We demonstrated also using an experiment that techniques employing the approximate trigonometric expansions for removing spectral correlation from multispectral imagery provides better results as compared to methods employing discrete cosine transform. In this section, we apply the approximate cosine expansion (ACE) to a multispectral imagery set for spectral decorrelation. Furthermore, the decorrelated image planes will be decomposed and represented by the approximated trigonometric expansions. For comparison purposes, the discrete cosine transform (DCT) will also be applied to the multispectral imagery set.

The multispectral imagery set under test consists of 10 bands each of spatial size 256x256 and 8 bits of resolution. Some sample images of the multispectral image set are shown in Fig. 3.10. The method applied for spectral decorrelation of the multispectral imagery is same as implemented in section 3.4. A 1-D vector from spectral correlated components from identical locations in each band is formed and an approximate cosine expansion applied on it. The resulting 1-D output vectors are placed adjacent to one another, in the same order as the input vectors, to form the stack of the spectrally decorrelated image planes. Fig. 3.11 shows first four spectrally decorrelated image planes associated with ten band multispectral test image set. For comparison purposes, discrete cosine transform was also applied on multispectral image set and decorrelated image planes were constructed. Since spectrally decorrelated bands are in floating point real numbers they must be quantized, to be subsequently coded by an image coding algorithm. For an 8-bit multispectral imagery, all decorrelated image planes can be linearly quantized into 8-bit images[38]. Although JPEG

based coding scheme could be used to code these decorrelated images, but the scheme would require modification of its parameters to suit the specific characteristics of the image set[38]. In chapter 3, we discussed capability of the approximate Fourier expansion to decompose signals using ideal bandpass filters. Now, we apply this decomposition to decorrelated image set using algorithm similar to Mallat's discrete wavelet transform discussed in [26], and implemented in section 3.5.

Since image plane 1 contains most of the energy, it can be linearly quantized to 12 bits[38]. After linearly quantizing all of the remaining decorrelated image planes into 8 bits, we applied the approximate Fourier expansion (AFE) for the purpose of decomposition of the decorrelated images. The decorrelated image planes were decomposed into 3 levels. In all, following actions were taken on the decorrelated and decomposed image planes:

1. Image planes 8,9 and 10 were set to zero.

2. Image plane 4, 5, 6 and 7 were subjected to following actions:

   i. The subimages $a01$, $a02$, and $a03$ of the first and the second decomposition level were set to zero.
   ii. The subimage $a03$ of the third decomposition level was set to zero.
   iii. The subimage plane $a00$, of size 32x32, was transformed using the approximate cosine expansion (ACE) with L equal to the size of the subimage. The number of retained coefficients, by threshold coding, was 730 of the total 32x32 coefficients.
   vi. The subimages $a01$ and a02 of the third decomposition level were transformed

using the approximate cosine expansion with L equal to the size of the subimage. The number of retained coefficients in each subimage plane was 128 of the total 32x32 coefficients in that subimage.

3. Image plane 2 and 3 were subjected to following actions:

   i. The subimages $a01$, $a02$, and $a03$ of the first and the second decomposition level were set to zero.
   ii. The subimages $a01$ and a02 of the third decomposition level were transformed using the approximate cosine expansion with L equal to the size of the subimage. The number of retained coefficients in each subimage plane was 256 of the total 32x32 coefficients in that subimage plane.
   iii. The subimage plane $a03$, of size 32x32, was transformed using the approximate cosine expansion (ACE) with L equal to size of subimage. The number of retained coefficients, by threshold coding, was 129 of total 32x32 coefficients.

The total number of coefficients/samples retained in all of the decomposed image planes came out to be 72819 of the total 256x256x10 samples in multispectral image set. Hence the total coefficient/sample reduction ratio (CRR) for ten band multispectral imagery came out to be:

$$C.R.R = \{int\}\frac{\text{Number of samples in image set}}{\text{Number of coeficients/samples retained in image set}} = \{int\}\frac{256x256x10}{72810} = 9 \qquad (4.4)$$

For reconstruction of the multispectral imagery, the process applied is inverse to that applied during decorrelation of multispectral image set, decomposition of each image plane and transformation of the subimages. The signal-to-noise-ratio of each reconstructed image in multispectral image set was computed and the result for first four bands is shown in Fig. 4.7. For comparison purposes, the block discrete cosine transform was applied on the image planes decorrelated by the discrete cosine transform. Following actions were taken on the image planes:

1. Image planes 8,9 and 10 were set to zero.

2. Image plane 4, 5, 6 and 7 were subjected to the following actions:

   i. The block discrete cosine transform was applied with block size of 16x16.
   ii. The number of retained coefficients was 385 of total 256x256 coefficients in each image plane.

3. Image plane 2 and 3 were subjected to the following actions:

   i. The block discrete cosine transform was applied with block size of 16x16.
   ii. The number of retained coefficients was 858 of total 256x256 coefficients in each image plane.

The total number of coefficients/samples retained in all of the decomposed image planes

came out to be 72819 of the total 256x256x10 samples in multispectral image set. Hence the total coefficient/sample reduction ratio (CRR) for ten band multispectral imagery came out to be 9. The method applied for reconstruction of the multispectral image set was similar as implemented in case of the approximate cosine expansion. The result for first four bands is shown in Fig. 4.8. It is clear from Fig. 4.7 and Fig. 4.8 that for multispectral image coding application, the approximate cosine expansion (ACE) yields higher signal-to-noise-ratio than discrete cosine transform (DCT).

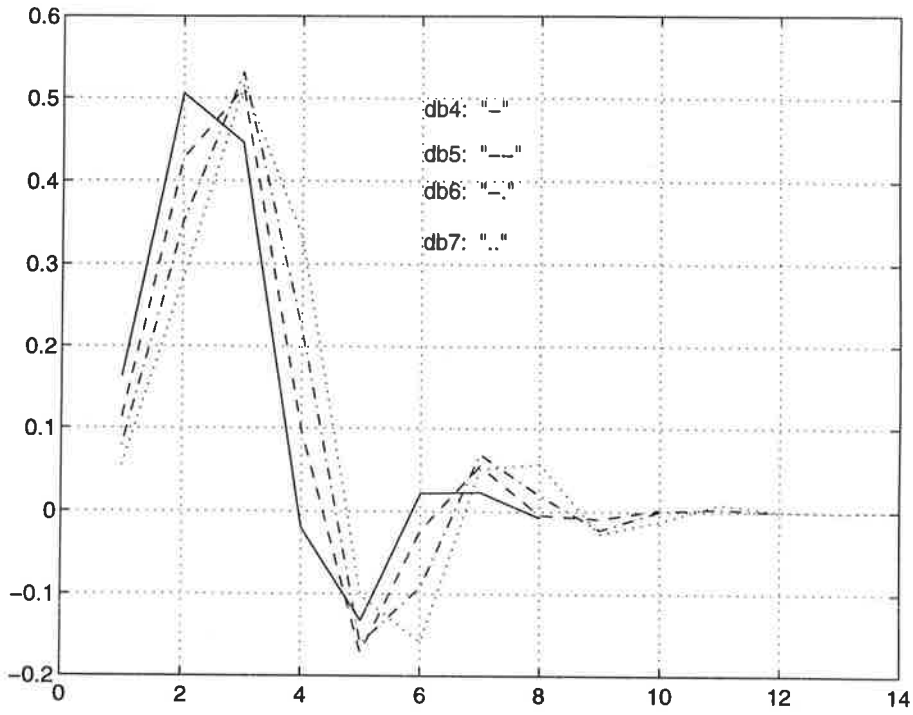

Fig. 4.1 Coefficients of some of the Daubechies filters

Fig. 4.2*a* Reconstructed "Lena" image using AFE, SNR_{ms}=14*dB*

Fig. 4.2*b* Reconstructed "Shipyard" image using AFE, SNR_{ms}=13.2*dB*

Fig. 4.3*a* Reconstructed "Lena" image using DCT, SNR_{ms}=32*dB*

Fig. 4.3*b* Reconstructed "Shipyard" image using DCT, SNR_{ms}=30.2*dB*

Fig. 4.4*a* Reconstructed "Lena" image using ACE, SNR_{ms}=34*dB*

Fig. 4.4*b* Reconstructed "Shipyard" image using ACE, SNR_{ms}=32.6*dB*

Fig. 4.5*a* Reconstructed "Lena" image using block DCT, SNR_{ms}=31.4*dB*

Fig. 4.5*b* Reconstructed "Shipyard" image using block DCT, SNR_{ms}=30*dB*

Fig. 4.6*a* Reconstructed "Lena" image using block ACE, SNR_{ms}=33*dB*

Fig. 4.6*b* Reconstructed "Shipyard" image using block ACE, SNR_{ms}=31.8*dB*

Fig. 4.7*a* Reconstructed "Lena" image using AFE/ACE, SNR_{ms}=35.6*dB*

Fig. 4.7*b* Reconstructed "Shipyard" image using AFE/ACE, SNR_{ms}=34.2*dB*

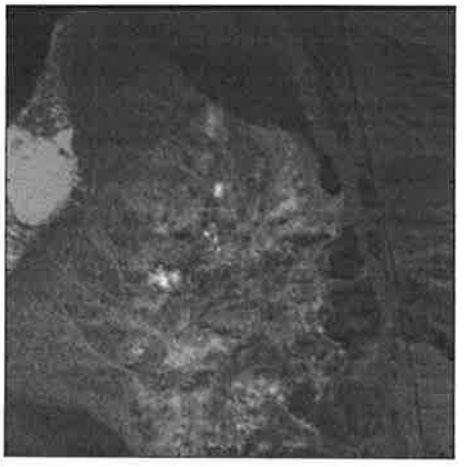

Fig. 4.8*a* Reconstructed band 1 using ACE, SNR_{ms}=34.5*dB*

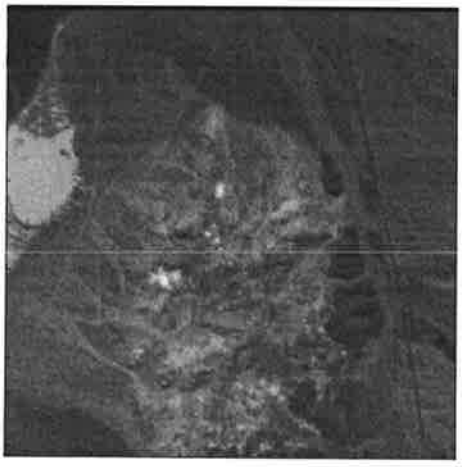

Fig. 4.8*b* Reconstructed band 2 using ACE, SNR_{ms}=35*dB*

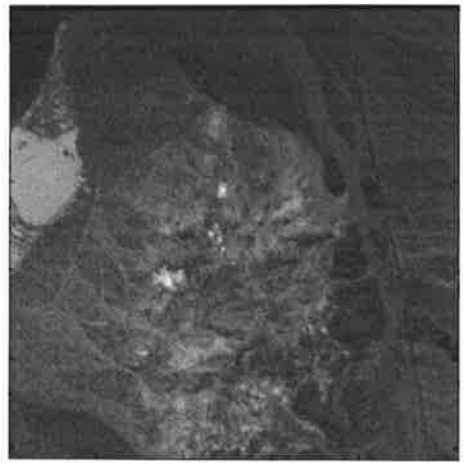

Fig. 4.8*c* Reconstructed band 3 using ACE, SNR_{ms}=34.7*dB*

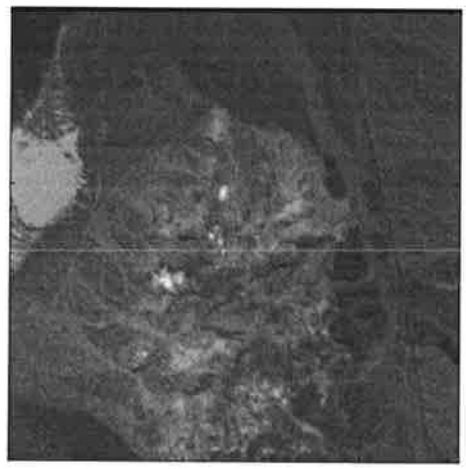

Fig. 4.8*d* Reconstructed band 4 using ACE, SNR_{ms}=35.2*dB*

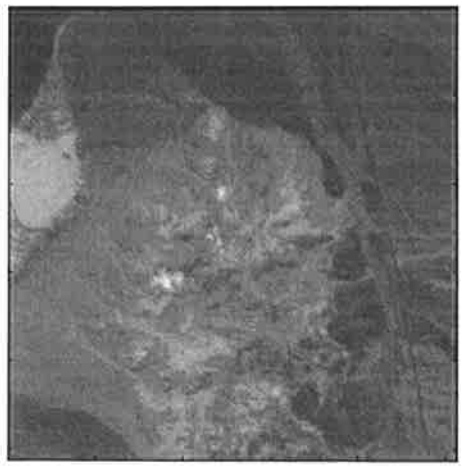

Fig. 4.9*a* Reconstructed band 1 using DCT, SNR_{ms}=34.2*dB*

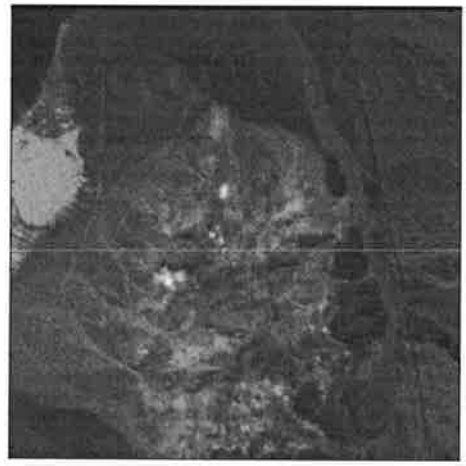

Fig. 4.9*b* Reconstructed band 2 using DCT, SNR_{ms}=33.2*dB*

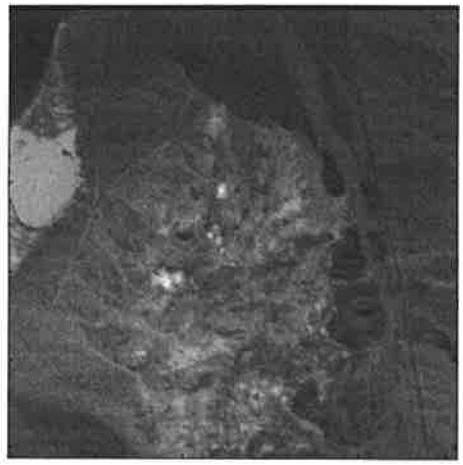

Fig. 4.9*c* Reconstructed band 3 using DCT, SNR_{ms}=32.9*dB*

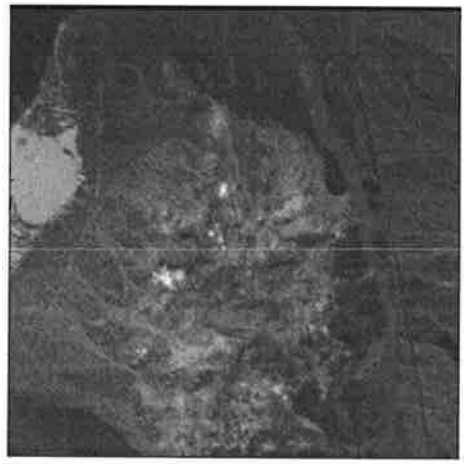

Fig. 4.9*d* Reconstructed band 4 using DCT, SNR_{ms}=33.3*dB*

5 . CONCLUSIONS

In this section, we summarize the contributions from this work, and propose some suggestions for the future research.

5.1 Summary of Contributions

The research reported in this thesis focused on the development and testing of a coding algorithm along with its comparative evaluation to existing conventional techniques employing discrete cosine transform (DCT) for the purpose of coding. The proposed technique provides an additional flexibility of signal decomposition in addition to its ability of signal representation in a constrained environment. Extensive simulations confirmed the improvement offered by the proposed technique over conventional techniques employing a single transform. In summary, following contributions were made:

1. In section 2.2, a discrete approximate Fourier expansion (AFE) for one dimensional, and non-periodic signals was proposed. Furthermore, some of the important properties of the discrete approximate Fourier expansion were derived, and it was shown that the discrete approximate Fourier expansion (AFE) yields relatively uncorrelated coefficients. In section 2.4, the mean square error between original and reconstructed signal (due to AFE) was computed. It was shown that mean square error of the reconstructed signal can be decreased if number of coefficients computed is larger than the length of the signal. This work is reported in [18-19].
2. In section 2.5, an approximate cosine expansion (ACE) was developed. It was shown

that for the same number of coefficients computed, the approximate cosine expansion (ACE) introduces less reconstruction error than the discrete approximate Fourier expansion (AFE) with the advantage that the coefficients are real. In section 3.4, the efficiency of the approximate trigonometric expansions was determined using the first order Markov process and it was shown that the spatial decorrelation, energy compaction and variance of coefficients of the approximate trigonometric expansions is better than the discrete cosine transform. This work has been reported in [19,21].

3. In section 3.3, the signal decomposition using the approximate Fourier expansion (AFE) was explored and it was shown that the filters other than the ideal bandpass characteristics can be used for signal decomposition. It was demonstrated that uniform or non-uniform signal decomposition can be achieved using the user-defined parameter of the approximate Fourier expansion (AFE). Performance in terms of signal decomposition and representation (in a constrained environment) was evaluated using speech signals in section 4.2 and images in section 4.4, and it was shown that the performance of the approximate trigonometric expansion is superior to that of the discrete cosine transform (DCT). This work is reported in [20,27].
4. In section 4.3, the approximate trigonometric expansions were applied to images for the purpose of coding. Based on local statistics of the image, the user-defined parameter L of the approximate Fourier expansion (AFE) can be varied for the purpose of signal decomposition and representation of the image blocks. It was shown using testing of various images that the images coded using the approximate trigonometric expansions yield higher signal-to-noise-ratio than the images coded using the discrete cosine transform (DCT). Furthermore, the compression achieved using the approximate trigo-

nometric expansions would be higher than using the discrete cosine transform (DCT) since the transformation efficiency of the approximate trigonometric expansion is superior to that of the discrete cosine transform for the first order Markov process. This work is reported in [19,21,].

5. In section 3.4, we applied an approximate cosine expansion (ACE) to the multispectral imagery for removing the spectral correlation from the multispectral image set. It was demonstrated that the spectral decorrelation efficiency as well as energy compaction of the approximate cosine expansion (ACE) is better than that of the discrete cosine transform (DCT). In section 4.4, we applied the approximate trigonometric expansions to the multispectral imagery for the purpose of coding, and it was shown that the signal-to-noise-ratio of the reconstructed multispectral image set was higher than that of the reconstructed multispectral image set tested using discrete cosine transform (DCT). This work has been reported in [39].

Apart from the research reported in this dissertation, considerable research has been done regarding impulsive suppression from images and direct-sequence spread-spectrum systems using rank order filters. This work is reported in [40-42].

5.2 Suggestions for Future Research

The scope of future research using multiresolution decomposition and representation techniques is very large. Future research using the approximate trigonometric expansions will focus on development of practical coding systems using the capabilities offered by the expansions. Specific research tasks using these expansions are as follows:

1. This thesis research explored the capability of the approximate trigonometric expansions for signal representation and coding using ideal bandpass filters. Different filters such as Gaussian or Daubechies filters can be used instead of ideal band pass filters to overcome the inherent limitations of the ideal bandpass filters.

2. In order to remove the windowing effect from the reconstructed signal, a post reconstruction strategy can be explored using adaptive signal processing techniques.

3. There is a great temptation to use a correlation reducing procedure in the temporal direction in addition to the spatial plane to increase the overall efficiency of the coding process. Therefore, a logical step is to extend the operation to a further, mutually perpendicular, direction, and to carry out three-dimensional transform coding employing the approximate trigonometric expansions. A strategy can be devised to explore the possibility of using the approximate trigonometric expansions in interframe coding of images.

4. The proposed technique can be applied to new applications such as color image representation and coding.

5. The future research can be directed to mixed approximate trigonometric expansion/transform of the signals using different filters.

6. The biorthogonal wavelet transforms have widely been us

ed for signal decomposition and synthesis due to their symmetry properties. The biorthogonal

wavelet transform allows the use of symmetric (even or odd) wavelets having compact support. Either wavelet can be used for the decomposition, provided that the other one is used for the reconstruction. The different filters leading to wavelets which are duals of each other, can be researched leading to biorthogonal approximate trigonometric expansion of the signal.

7. Considerable research can be done in extending the approximate Fourier expansion (AFE) to higher order spectral analysis.

6 . REFERENCES

[1] C.E. Shannon,"A Mathematical Theory of Communication", *Bell System Tech. Journal*, 27:379-423,623-656, 1948.

[2] N.J.A Sloane and A.D. Wyner,eds., *Claude Elwood Shannon, Collected Papers*, IEEE Press, NewYork, 1993.

[3] R.G. Gallager, *Information Theory and Reliable Communication*, NewYork: John Wiley, 1968.

[4] C.E. Shannon and W. Weaver, *The Mathematical Theory of Communication*, Urbana, The University of Illinois Press, 1949.

[5] J. Ziv and J. Lemple,"A Universal Algorithm for Sequential Data Compression", *IEEE* Trans. Info. Theory, IT-23(3):337-343, 1977.

[6] J. Ziv and J. Lemple,"A Universal Algorithm for Sequential Data Compression", *IEEE Trans. Info. Theory*, IT-24(5):337-343, 1977.

[7] D.A. Huffman,"A Method for the Construction of Minimum Redundancy Codes", *Proc. IRE*, 40(10):1098-1101, 1952.

[8] J.S. Vitter,"Design and Analysis of Dynamic Huffman Codes",*Journal of the ACM*, October 1987.

[9] M.R. Nelson,"Arithmetic Coding and Statistical Modelling", *Dr. Dobbs' Journal*, February 1991.

[10] M. Rabbani and P.W. Jones,"*Digital Image Compression Techniques*",SPIE, 1991.

[11] W.Penebaker and J.Mitchel,"*JPEG Still Image Compression Standard*", Van Nostrand Reinhold, NewYork, 1992.

[12] ISO/IEC DIS 10918-1,"*Digital compression and coding of continuous-tone still images*", Jan 2, 1992.

[13] ISO/IEC Int'l Standard IS 11172-3,"*Information Technology-Coding of Moving Pictures and Associated Audio for Digital Storage Media at up to about 1.5 Mbits/s-Part3:Audio*".

[14] V.D. Vaughn and T.S. Wilkinson, "System Considerations for Multispectral Image Compression Designs", *IEEE signal processing magazine*, pp. 19-31, January 1995.

[15] A. K. Jain, "Image data Compression: A Review", *Proceedings of the IEEE*, pp. 349-389, Vol. 69, No. 3, March 1991.

[16] A. K. Jain, " A sinusoidal family of unitary transforms", *IEEE Trans. Pattern Anal. Machine Intell.*, vol. PAMI-1, pp. 356-365, Oct. 1979.

[17] A. Papoulis, "*Probability, Random variables, and Stochastic Processes*", McGraw-Hill Book Company, New York, 1965.

[18] Q. Memon, T. Kasparis, N. Tzannes, "An Approximate Fourier Expansion with uncorrelated coefficients", *IEEE Mediteranean Symposium on Advancements in Controls*", June, 1995.

[19] Q. Memon, T. Kasparis,"Transform Coding of Signals using Approximate Trigonometric Expansions", Submitted to *Journal of Electronic Imaging*.

[20] Q. Memon, T. Kasparis,"Adaptive Transform Coding of images using Approximate Trigonometric Expansions", *Proceedings of International Photonics East '96 Symposium*, vol. 2915, No. 07, 18-21 November, Boston, MA, 1996.

[21] Q. Memon, T. Kasparis,"Approximate Trigonometric Expansions with applications to image encoding", *Proceedings of SPIE International Aerosense symposium*, vol. 2751,

No. 3, pp. 26-35, April 08-12, Orlando, 1996.

[22] P.J. Burt and E.H. Adelson,"The Laplacian pyramid as a compact image code, *IEEE Trans. Commun.*, COM-31, pp. 532-540, 1983.

[23] D. Esteban and C. Galand,"Application of Quadrature Mirror Filters to split-Band Voice Coding System", *International Conference on Acoustics, Speech and signal Processing*, Washington, DC, pp.191-195, 1977.

[24] J.W. Woods and S.D. O'Neill,"Subband Coding of Images", *IEEE Transactions*, ASSP-34:1278-1288, 1986.

[25] A. Croisier, D. Esteban, and C. Galand,"Perfect Channel Splitting by use of Interpolation, Decimation, Tree Decomposition Techniques", *International Conference on Information Sciences and Systems*, pp.443-446, 1976.

[26] S. Mallat,"A Theory for Multiresolution Signal Decomposition:The Wavelet Representation", *IEEE Transactions.*, PAMI-11:674-693, 1989.

[27] Q. Memon and T. Kasparis,"Application of Approximate Trigonometric Expansions to Multiresolution Signal Representation", *Proceedings of IEEE Southcon'96*, pp. 308-313, June 25-27, 1996.

[28] A. Akansu and R. Haddad, "*Multiresolution signal decomposition, Transforms, Subbands, Wavelets*", Academic Press Inc., CA, 1992.

[29] R. J. Clarke, "*Transform Coding of Images*", Academic Press Inc., London Ltd., 1985.

[30] N. Ahmed, T. Natarajan, and K. R. Rao, "Discrete Cosine transform", *IEEE Trans. Comput.* C-23, pp. 90-93, 1974.

[31] J. Pearl, H.C Andrews, and W.K Pratt, "Performance measures for transform data coding," *IEEE Trans. Commun. Technol.*, vol. COM-20, pp.441-415, June 1972.

[32] R. J. Clarke, "*Digital Compression of Still Images and Video*", Academic Press Inc., CA. , 1995.

[33] I. Daubechies, "*Ten lectures on wavelets*", SIAM, 1992.

[34] I. Daubechies, "Orthonormal Bases of Compactly Supported Wavelets", *Comm. in Pure and Applied Math.*, vol. 41, pp. 909-996, 1988.

[35] I. Daubechies, "The Wavelet Transform, Time-Frequency Localization and Signal Analysis", *IEEE Transactions on Information Theory*, vol. 36, pp. 961-1005, Sept. 1990.

[36] R. Gonzalez and R. Woods, "*Digital Image Processing*", Addison-Wesely Publication Company, Massachusettes, 1992.

[37] N. Jayant and P. Noll, *Digital Coding of Waveforms*, Prentice Hall, Inc. 1984.

[38] J. Saghri, A. Tescher and J. Reagan,"Practical Transform Coding of Multispectral Imagery," *IEEE Signal Processing Magazine*, pp. 32-43, January 1995.

[39] Q. Memon, T. Kasparis, "An Efficient Algorithm for Multispectral Data Coding using Approximate Trigonometric Expansions", *Proceedings of SPIE's AeroSense Symposium*, vol. 6201, No. 528, April 21-25, Orlando, 1997.

[40] T. Kasparis, M. Georgiopoulos, Q. Memon, "Direct-Sequence Spread-Spectrum with Transform Domain Inteference Suppression", *Journal of Circuits, Systems, and Computers*, Vol. 5, No. 2, pp. 167-179, 1995.

[41] Q. Memon, T. Kasparis, "Block Median Filters", *Proceedings of SPIE's AeroSense Symposium*, Vol. 2488, pp. 100-109, Orlando, 1995.

[42] T. Kasparis, Q. Memon, R. Koteswaran, "Rank Filters with Adaptive Length", *Proceedings of SPIE's AeroSense Symposium*, Vol. 2239, pp. 256-266, Orlando, 1994.